ISSN 0389-4010
UDC 662.61

TECHNICAL REPORT OF NATIONAL AEROSPACE LABORATORY

TR-1318T

Numerical Studies of Swirling Turbulent Flows in Conventional and DS Burners

Yan LIU, and Shigeru HAYASHI

January 1997

NATIONAL AEROSPACE LABORATORY

CHOFU, TOKYO, JAPAN

Numerical Studies of Swirling Turbulent Flows in Conventional and DS Burners*

Yan LIU*[1] and Shigeru HAYASHI*[2]

ABSTRACT

In this paper, the effects of swirler configurations on the turbulent flows and fuel-air mixing process in a swirl burner are investigated by numerical simulations. The configurations studied are a unique double swirler (DS) which is designed for low-NO_x emissions, and two conventional single swirlers with different hub diameters and the same opening area. The double-swirler has a pair of co-rotational swirls and a convergent duct. One of them is attached to the inlet of the duct and the other is externally and concentrically attached to the duct at the exit. Combustion air flows into a flame tube through both duct and the annular passage of the outer swirler. In the conventional swirlers, combustion air flows through the annular passage with swirl vanes.

The study is performed using a finite volume formulation. A body-fitted non-orthogonal grid system is specially generated for predicting flows in the double swirler. In the study, three different turbulent models, e.g., the standard κ-ε model, RNG κ-ε model, and Reynolds Stress Model (RSM), are used to calculate turbulent properties in the flow, and their predictive abilities are assesed and compared to each other. The flow characteristics in the burners and their variations with the inlet flow conditions are then analyzed numerically.

The results in this study indicate that these three different turbulent models all give general flow characteristics of the swirling flows considered in this work, but show different predictions of the size of central toroidal recirculation zone (CTRZ), mainly in the downstream of the flow. The experimental evaluation conducted for the flow in the DS burner indicates that the predicted CTRZ sizes given by the standard κ-ε model show comparatively good agreement with the experiment data, while the RNG κ-ε model predicts the rigid vortex motion in the strongly swirling flow more accurately. It is found from the predictions conducted for the conventional burners that the RSM model is also able to improve the prediction of the rigid vortex motion. The study of the effects of inlet conditions on flow patterns reveals that the double swirler possesses unique advantages over conventional swirlers, e.g., the flow pattern as well as the fuel concentration distribution in the burner could actually be controlled by changing the ratio of the air flow rate in the inner and outer swirlers or the fuel flow rate through the fuel nozzle. A high-velocity jet is produced near the exit of the double swirler, and it may enhance the mixing process of the air and fuel due to opposing effect of the jet and the reverse flow in the burner. The flow patterns in the burners with conventional swirlers of different hub diameters, on the other hand, are similar, and they do not change significantly with variation of the inlet conditions when the swirler vane angle remains the same. The difference in the swirler hub diameters, however, changes the size of CTRZ. The smaller hub may decrease the width of CTRZ in the burner.

Key Words: swirling flow, turbulent models, numerical calculation, burner, fuel-air mixing

---

* Received 1 January 1997
*[1] STA Fellow
*[2] Reacting Flow Research Laboratory, Thermofluid Dynamics Division

従来型スワーラと新規なダブルスワーラを備えたバーナの旋回乱流流れの数値計算

－非燃焼時の流れと燃料濃度分布－

バーナ内の乱流と燃料－空気の混合過程に及ぼすスワーラの形態の影響を数値計算により調べた。対象とした形態は，開口面積，羽根角は同じで，ハブ径が異なる2個の従来型スワーラと1個の新規なダブルスワーラ (DS)とである。このダブルスワーラは，同方向旋回の一対のスワーラと縮小ダクトで構成される。1個のスワーラはこのダクトの入り口に，また，他の1個はダクト出口部において，それと同軸に外側から取り付けられていて，燃焼空気はダクトと外側スワーラとから燃焼筒に流入する。これに対して，従来型のスワーラでは，ハブと同軸の環状通路だけから空気が流入する。

数値計算には有限体積法を用いた。空気通路が曲面で形成されたダブルスワーラの流れの予測には物体適合非直交格子を生成させた。流れの乱流特性を計算するために3種類の乱流モデル，標準 κ-ε モデル，RNG κ-ε モデル，およびレーノルズ応力モデルを用い，それらの予測性能を比較・評価した。バーナ内の流れ特性と，入り口条件の変化に対するその変化を数値的に分析した。

3種類の乱流モデルは，どれもこの研究で対象とした旋回流れの一般的な特性を予測できたが，中心のトロイダル循環流領域 (CTRZ) の大きさには，特に下流において，差が生じた。DS バーナの流れについては，実験との比較から，標準 κ-ε モデルによる CTRZ の大きさは実験データと比較的よく合うこと，RNG モデルは強い旋回流れ中の剛体渦運動の予測を改善することができることが分かった。RSM モデルは，従来型スワーラによる剛体渦運動の予測を改善することができることも分かった。

流れパターンに与える入り口条件の影響についての研究から，このダブルスワーラは従来型スワーラに比べて特徴的な利点，すなわち，バーナ内の流れパターンと燃料濃度分布が，内・外スワーラへの空気流量比あるいは燃料ノズルの燃料流量を変えることによって制御できることが分かった。ダブルスワーラの出口近傍に高速の噴流が形成され，この噴流と燃焼器内の逆流との対向によって空気と燃料の混合が促進される。従来型スワーラの流れパターンは類似で，スワーラの旋回角が一定なら入口条件によって著しく変化することはなかった。CTRZ の大きさはスワーラのハブ径によって変化し，ハブ径が小さいと CTRZ も小さかった。

1. Introduction

A series of experimental studies have been conducted on a double swirler burner as well as conventional swirler burners [1] [2], as a part of the effort to reduce the NOx emissions from gas turbines and propulsion engines. From gas temperature and NOx measurements, it was found that the combustion was more complete in the direct injection combustion systems employing the double-swirler burner than in premixed-prevaporized combustion systems while keeping very low NOx emissions, and that the burner with the double swirler could produce lower NOx emissions than the conventional burners. For a further understanding of the physical processes in those burners, the revelation of the detailed flow characteristics in the burners is required. It is for this reason that the numerical simulations of the swirling turbulent flows in the burners are being carried out in this paper.

In combustion systems, swirling flows have been extensively adopted as effective means of providing aerodynamic controls in stabilizing the flame, enhancing fuel-air mixing and heat transfer, and abating the pollutants. Extensive reviews on the phenomena and application of swirling flow can be found in [3] [4] and [5].

Swirling motion is the result of an impartation of the tangential velocity component by use of a swirl generator positioned upstream of the flow field, and the swirling turbulent flows with sufficient intensity are generally considered to be complex in nature [5].

In principle, there is no need to adopt special practices for turbulent flow, for the Navier-Stokes equations apply equally as to a laminar one. However, although the advent of the supercomputer permits Direct Numerical Simulation of turbulent motion in simple geometry, this is not a practically possible route for engineering application of today yet. Instead, the

time-averaged decompositions are commonly used for the conservation equations of turbulent flows, but there is no direct way to estimate the magnitudes of statistical correlation in the averaged equations. The turbulence closure problem occurs in order to supply the information missing from the averaged equations.

Based on the consideration of applicability, accuracy, simplicity, and economy of computer effort, quite a few turbulence-models-associated phenomenological conjectures have been proposed for the simulation of turbulent flow. These models have been described in several excellent review papers, for instance, in [6]. Among these models, one successful two-equation model, the standard κ-ε turbulence model, has been widely applied to engineering practice, but has been described as being unsatisfactory in simulation of strongly swirling flows [5-8]. The deficiency of the standard κ-ε model stems perhaps from the neglect of anisotropic viscosity and additional turbulence generation arising from the effects of streamline curvature [6] [9]. Many modified κ-ε turbulence models, taking into account the enhanced turbulent diffusion caused by extra strain rates incorporated with streamline curvature have thus been proposed [5, 6, 10]. The modified κ-ε models, however, were still not able to yield satisfactory predictions of swirling flows with the swirl intensities from low to high extents [5, 7]. Recently, the further development of the Renormalization Group (RNG) provides a better methodology for the turbulence models [11]. The RNG κ-ε model, which is derived mathematically, is claimed to be free from any empirically adjustable parameters. Although the RNG turbulence model has been successfully used in calculating wake flow, boundary flow, etc., it appears that more studies need to be done to evaluate the model against experimental data for swirling flow simulation.

An attractive alternative is the use of higher-order turbulence closure models such as the Algebraic Stress Models (ASM) and the Reynolds Stress Models (RSM). Many studies [5-7] reported, however, that in swirling recirculating flows, the improvements of flow field predictions using the ASM were not so pronounced in comparison with those using κ-ε models. Ref. [12] pointed out further that the ASM hypothesis seriously misrepresented the diffusive transport of the stress components and this was aggravated by a failure accounting for additive swirl-related stress transport terms in the algebraic modeling process. For highly anisotropic flows such as swirling recirculating case, the RSM has been demonstrated to be capable of reproducing, to a certain extent, the major features of the flows, [12-15], but it greatly increased the computational complexity and time requirement. Furthermore, the fact remains that as the order of the turbulence model is increased, the number of empirical constants increases, and insufficient model assessments lead to less generality of these empirical constants in applications [15]. So it seems that the choice of the turbulence models in the simulation of swirling flows is still an argumentative topic.

The present work, in addition to the study of the variations of the inlet flow conditions on the flow patterns in the burners, also employs different turbulence models, e.g., the standard κ-ε model, the RNG κ-ε model, as well as the Reynolds Stress Model, to study their predictive abilities in the calculation of swirling turbulent flows.

In the following, the mathematical formulation and numerical procedure are described firstly in section 2, the calculation results and discussion are then presented in section 3, and some conclusions are finally summarized in section 4.

2. Mathematical Formulation and Numerical Procedure

2.1 Description of the Problem

The flow system for which the present simulation is conducted is shown in Fig. 1. It mainly consists of an upstream swirler set and a flame tube 300 mm in length and 80 mm in diameter. In the swirler set, three different swirlers shown in Fig. 2 are used separately, one being a double swirler, and the others being conventional single swirlers with different hub diameters. The two swirlers in the double swirler are co-rotational, each has 16 curved vanes with an angle of 45 degrees. The swirlers are concentric but offset. The swirlers are mounted at either end of a converging duct. The one is located on the inside of the duct at the upstream end, and the another on the outside of the duct at the narrower, downstream end. The entering

air is splitted between the duct and the annular passage of the outer swirler with a ratio of 1:2. The convergent duct is designed to form a high velocity jet [1]. The conventional swirlers, on the other hand, are the same in respect to opening area, but different in hub diameters (for convenience, hereafter in this paper, DS will be used to stand for the double swirler, SS for the conventional swirler with a smaller hub, and LS for the conventional swirler with a larger hub). The nominal swirl numbers for the small-hub and large-hub swirlers are 0.8 and 0.88 respectively, which might form a "strong" swirl, according to the criterion given in [16].

The DS burner, which uses the double swirler, is followed by a divergent cone and then by a flame tube, as shown in Fig. 1, while the conventional burners, which use single swirlers, are mounted flush to the end plate of the flame tube. Multi-hole fuel nozzles are employed in all burners to inject gaseous fuel (methane) into the air flow at angle of 60 degrees for the DS burner and 120 degrees for the conventional burners. They are placed co-axially with the swirlers. In the present study, the temperature of the entering air was kept at 350K, and the flow in the combustor is isothermal.

2.2 Governing Equations and Turbulence models

By performing the Reynolds decomposition and time averaging, the instantaneous conservation equations can be transformed into a system of equations commensurate with turbulent flow computations. For brevity, the governing equations for continuity, momentum and species are given here in the form of the Cartesian notation with the assumptions of steady state and a Newtonian fluid:

$$\frac{\partial}{\partial x_j}\rho u_j = 0 \tag{1}$$

$$\frac{\partial}{\partial x_j}(\rho u_j u_i) = -\frac{\partial p}{\partial x_i} + \frac{\partial}{\partial x_j}\left[\mu\left(\frac{\partial u_j}{\partial x_i} + \frac{\partial u_i}{\partial x_j}\right)\right] - \frac{\partial}{\partial x_j}(\rho\overline{u'_j u'_i}) - \frac{2}{3}\frac{\partial}{\partial x_i}\left[\mu\left(\frac{\partial u_j}{\partial x_j}\right)\right] + \rho g_i \tag{2}$$

$$\frac{\partial}{\partial x_j}(\rho u_j m_i) = \frac{\partial}{\partial x_j}\left(\Gamma\frac{\partial m_i}{\partial x_j}\right) - \frac{\partial}{\partial x_j}(\rho\overline{u'_j m'_i}) + R_i \tag{3}$$

Where μ is the dynamic viscosity of the fluid, Γ is the diffusivity of species, and R_i is the mass rate of creation or destruction by chemical reactions, and the double correlation $\rho\overline{u'_j m'_i}$ in Eq. (3) is approximated by:

$$\rho\overline{u'_j m'_i} = \Gamma_t\frac{\partial m_i}{\partial x_j} \tag{4}$$

The $\rho\overline{u'_j u'_i}$ in Eq. (2) are the Reynolds stresses, and they must be related to turbulence models. As mentioned in section 1, currently there exist many turbulence models for the swirling turbulent flows. In the present paper, three turbulence models, e.g., the standard κ-ε model, the RNG κ-ε model, and the Reynolds Stress Model (RSM) are to be used in the prediction.

The Standard κ-ε Model

The Boussinesq hypothesis states that the Reynolds stress is proportional to the mean velocity gradient, and the constant of the proportionality is denoted "turbulence" or "eddy" viscosity, that is:

$$\rho\overline{u'_j u'_i} = \frac{2}{3}\rho\kappa\delta_{ij} - \mu_t\left(\frac{\partial u_i}{\partial x_j} + \frac{\partial u_j}{\partial x_i}\right) \tag{5}$$

Based on Eq. (5) and the Prandtl-Kolmogorov relation, the transport equations for κ and ε in the κ-ε model are described as follows [17]:

$$\frac{\partial}{\partial x_j}(\rho u_j\kappa) = \frac{\partial}{\partial x_j}\left(\frac{\mu_t}{\sigma_k}\frac{\partial\kappa}{\partial x_j}\right) + H_k \tag{6}$$

$$\frac{\partial}{\partial x_j}(\rho u_j\varepsilon) = \frac{\partial}{\partial x_j}\left(\frac{\mu_t}{\sigma_\varepsilon}\frac{\partial\varepsilon}{\partial x_j}\right) + H_\varepsilon \tag{7}$$

the source terms are:

$$H_\kappa = -\rho\varepsilon - \rho\tau_{ij}S_{ij} \tag{8}$$

$$H_\varepsilon = -\rho C_1\frac{\varepsilon}{\kappa}\tau_{ij}S_{ij} - \rho C_2\frac{\varepsilon^2}{\kappa} \tag{9}$$

where σ_κ, σ_ε, C_1, C_2 are constants (1.0, 1.3, 1.44, and 1.92 respectively). The values of these constants are the standard ones suggested by Launder and Spalding [17].

The eddy viscosity μ_t is calculated via the relationship:

$$\mu_t = \rho C_\mu\frac{\kappa^2}{\varepsilon} \tag{10}$$

where $C_\mu = 0.09$.

The shortcomings of the standard κ-ε model are: (1) the model is empirically based; (2) it cannot be extended to low Reynolds number flows; (3) the κ and ε equations cannot be integrated to the wall, so wall functions are needed; (4) it assumes isotropicity for the eddy viscosity.

RNG κ-ε Model

The RNG κ-ε model is derived from the Renormalization Group theory [11]. In this new turbulence model, the κ equation is the same as that in the standard model but the source term in the ε equation is now given by the following expression:

$$H_\varepsilon = -\rho C_1 \frac{\varepsilon}{\kappa} \tau_{ij} S_{ij} - \rho C_2 \frac{\varepsilon^2}{\kappa} - \rho R \qquad (11)$$

The extra term, R, the rate of strain, is as follows:

$$R = \frac{C_\mu \eta^3 (1 - \eta/\eta_0)}{1 + \beta \eta^3} \frac{\varepsilon^2}{\kappa} \qquad (12)$$

where $\eta = \frac{\kappa}{\varepsilon} (2 S_{ij} S_{ij})^{1/2}$, $\eta_0 = 4.38$, and $\beta = 0.015$.

The coefficients derived from the RNG theory are C_1=1.42, C_2= 1.68 and $\sigma_\kappa = \sigma_\varepsilon = 0.72$, and the effective viscosity μ_{eff} in the RNG κ-ε model is computed by the following expression:

$$\mu_{eff} = \mu \left[1 + \sqrt{\frac{\rho C_\mu}{\mu}} \frac{\kappa}{\sqrt{\varepsilon}} \right]^2 \qquad (13)$$

The RNG κ-ε model is derived from theory, so it is valid over the region from high to low Reynolds number and can be integrated to the wall. It is believed that the strain term in the more fundamentally treated ε equation may give improved predictions for ε in regions of high strain, and consequently lead to a more realistic value for κ, and together these should yield an improved prediction for μ_t. The μ_t, however, is still a scalar according to equation (13).

The Reynolds Stress Model (RSM)

Different from the κ-ε models which assume isotropic eddy viscosity, the RSM model predicts components of the Reynolds stresses directly and could duplicate the flow characteristics associated with anisotropy, curvature, etc. The RSM uses the following differential equations in which the modeling assumptions of Ref. [15] have been used to provide closure:

$$\frac{\partial}{\partial \chi_k} (\rho u_k \overline{u'_i u'_j}) = D_{ij} + \rho P_{ij} + \rho \Phi_{ij} - \frac{2}{3} \delta_{ij} \rho \varepsilon \qquad (14)$$

$$D_{ij} = C_s \frac{\partial}{\partial \chi_k} \left(\rho \frac{\kappa}{\varepsilon} \overline{u'_k u'_l} \frac{\partial \overline{u'_i u'_j}}{\partial \chi_l} \right) \qquad (15)$$

$$P_{ij} = -\left(\overline{u'_k u'_j} \frac{\partial u_i}{\partial \chi_k} + \overline{u'_i u'_k} \frac{\partial u_j}{\partial \chi_k} \right) \qquad (16)$$

$$\Phi_{ij} = -C_1 \frac{\varepsilon}{\kappa} (\overline{u'_i u'_j} - \frac{2}{3} \kappa \delta_{ij}) - C_2 (P_{ij} - \frac{2}{3} P \delta_{ij}) \qquad (17)$$

Where the model constants C_s, C_1, C_2 are 0.24, 1.8, and 0.6 respectively.

In the case of swirling flows, 6 differential equations for the individual Reynolds stresses have to be solved to close the turbulent properties.

2.3 Computational Method and Boundary Conditions

The differential equations in the last section, which are highly nonlinear and strongly coupled, will be solved by utilizing the finite volume method [18], in which a finite volume formulation of equations that are derived by integration of the differential equations over control volumes of finite size is employed. The solution procedure used is the SIMPLE algorithm [19], which is based on the following features:

(1) Solve the momentum equations, based on the current guess for pressure, p^*, to update velocities, u, v, w.
(2) Solve the mass balance equation, in pressure-correction form, to update velocity and pressure.
(3) Solve all scalar equations (species, κ, ε).
(4) Solve auxiliary equations (e.g. RSM).
(5) Update fluid properties.
(6) Repeat (if unconverged).

The equations are solved sequentially via a line by line (TDMA) process, underrelaxtion factors are used for iteration to help the convergence. The factors are changed in the process of calculation, they are also changed with different turbulence models.

In this work, the fact that the configuration of the DS swirler is complicated, the size is small, and the inner wall of the duct is curved requires the use of body-fitted-coordinates in the solution. In the case of the DS burner simulation, the governing equations are transformed into the ones in general non-orthogonal

co-ordinates. Two steps are needed to perform the transformation. The first step is to transform the flow area in the physical plane into a parallelogram in a computation plane according to the general transformation, which is generated by an algebraic/elliptic method [20]. The second step is to transform the governing equations in the computational plane while maintaining the same dependent variables. The resulting governing equations are then solved by the same solution procedure described above.

Due to the elliptic nature of the governing equations, boundary conditions should be specified at all the boundaries of the computational domain, including the inlet, outlet, confined wall and symmetric axis boundaries. In the present study, the following boundary conditions have been applied.

At the inlet:

(a) Axial velocity U_{in} for air is assumed uniform and computed from the mass flow rate of air, and for the DS burner, the flow rate is splitted between inner and outer swirlers.

(b) Radial velocity $V_{in} = 0$.

(c) Tangential velocity $W_{in} = U_{in} \tan\theta$, θ is the swirler vane angle.

(d) The turbulent quantities are set as:

$$\kappa_{in} = (0.05U_{in})^2, \ \varepsilon_{in} = \frac{0.16\kappa_{in}^{3/2}}{0.2L}$$

where L denotes the inlet radius [17].

For the RSM model, the Reynolds stresses are given as:

$$\overline{u'^2_i} = \kappa, \ \overline{u'^2_j} = \overline{u'^2_k} = \frac{1}{2}\kappa, \ \overline{u'_i u'_j} = 0.0$$

(e) For fuel mass fraction,

$m_{fu} = 0$ in the region of air inlet,

$m_{fu} = 1$ in the region of fuel injection.

The velocity components for gaseous fuel (from fuel nozzle) is determined from the fuel mass flow rate and the injection angle. The fuel is injected from an annulus with the same area as the total area of all individual holes of the nozzle.

On the centerline:

The conditions which have to be satisfied are:

(a) No cross-flow.

(b) Zero diffusion flux of the variables in the direction normal to the axis of symmetry.

On the wall:

The boundary conditions for the wall are set by using the standard wall functions [17]. The approach relates the velocity components as well as turbulent quantities to the friction velocity, which is obtained from the log-law for the flows near a wall.

At the outlet:

The flow at the exit are assumed to be fully developed, so the diffusion flux of the variables in the axial direction equals to zero.

2.4 Grid System and Calculation Conditions

The numerical calculation domain and grid system used for the LS burner are shown in Fig. 3. The grid size contracts in the radial direction and expands in the axial direction from the sudden expansion towards the exit, hence finer grid spacing is formed near the burner walls. In the present computation, a 189 x 50 grid system with 0.95 contraction in the radial direction and 1.05 expansion in the axial direction is employed. The grid system is chosen to be very fine because of the requirement of accurate processing of boundary conditions as well as the desire for detailed flow characteristics. The similar grid arrangements are used for the SS burners. The position for air inlet, however,

Table 1 Simulation Conditions Burners

Burners	M_t (g/s)	M_1 (g/s)	M_2 (g/s)	M_f (g/s)	Cases
DS	25.10	8.37	16.73	0.77	1*
	50.20	16.73	33.47	0.77	2
	50.20	33.47	16.73	0.77	3
	50.20	25.10	25.10	0.39	4
	50.20	25.10	25.10	0.77	5
	50.20	25.10	25.10	1.54	6
	100.40	50.20	50.20	0.77	7
LS	25.10	25.10	—	0.77	8*
LS	50.20	50.20	—	0.77	9
SS	25.10	25.10	—	0.77	10

* Experiments were conducted for these cases.

M_t: total air flow rate;

M_1: air flow rate entering the inner swirler of the double swirler;

M_2: air flow rate entering the outer swirler of the double swirler;

M_f: fuel flow rate through the fuel nozzle.

is different due to the difference of swirler hub diameters.

The grid arrangement for the conventional burners is easy. The complicated configuration of the DS burner, however, requires the use of body-fitted-coordinates. In the present study, a grid system of total 230 x 50 grid nodes is used for the DS burner, as shown in Fig. 4. For the zones in the double swirler and the divergent cone, a body-fitted-coordinate's subsystem is generated by an algebraic/elliptic method, as shown in Fig. 5. The operating conditions of the burners for which numerical simulation is done and the corresponding case number are listed in Table 1.

3. Results and Discussion

3.1 Effects of Turbulence Models on Predictions

In this section, the basic flow patterns in the DS and conventional burners, the effect of turbulence models, as well as their experimental evaluation, where the experimental data are available, are to be presented and discussed.

3.1.1 DS Burner (Case 1)

Standard κ-ε model

Figure 6 presents the predicted results using the standard κ-ε model for Case 1, where the air mass flow rate in the second swirler is twice as that in the first swirler, that is $M_2 = 2M_1$. Figures 6(a) and (e) are the velocity vector and stream function distributions respectively, from which the flow pattern in the DS burner can be clearly observed. As expected, a central toroidal recirculation zone (CTRZ), which is the result of swirling motion, is formed in the front central region of the burner, and a corner recirculation zone (CRZ), that is formed by sudden expansion, is also produced in the corner of the flame tube. The size of CTRZ, which can be observed from the axial velocity distribution in Fig. 6(b), is less than half the total length of the burner. The distribution changes greatly in the front region, but gradually becomes fully developed at a certain distance in the downstream. The combined swirling effect from two swirlers, as indicated from the tangential velocity distribution in Fig. 6(c), forces the stream to flow close to the divergent cone wall, due to which a fuel distribution featured with two peaks is formed, as given in Fig. 6(d).

The vector velocity, the axial velocity, the tangential velocity and fuel concentration distributions in the double swirler are given in Figs. 7(a)-(d), which makes the observation of the flow pattern inside the DS possible. From Figs. 7(a) and (b), it can be seen that the converged duct makes the stream accelerate in a great rate, and forms a high speed stream jet at the exit. The maximum velocity occurs close to inner wall of the duct due to the swirling effect from the inner swirler. The reversed flow right behind the fuel nozzle is formed for two reasons: one is the low pressure zone caused by the existence of the nozzle, and the other is the swirling motion of the double swirler. The fact that the two swirlers in double swirler are co-rotational makes the swirling stronger, and the tangential velocity is, as shown in Fig. 7(c), quite large in the double swirler and the connecting divergent cone. Figure 7(d) shows that the fuel stream, which is injected at an angle of 60 degrees into the air stream from the first swirler, falls mainly into the high-velocity jet due to opposing effect of the jet flow from the double swirler and reverse flow. This makes the peak of fuel distribution occur in the main flow and forms good mixing in the combustor.

RNG κ-ε model

For the same case (Case 1), the predicted results using the RNG κ-ε model are shown in Fig. 8. Comparing with Fig. 6, it can be seen that the flow pattern given by the RNG κ-ε model is also characterized by a strong swirling flow, e.g., a small CRZ and a much longer CTRZ, and the corresponding velocity distributions are similar. With the RNG κ-ε model, however, there are some changes in the details of the flow field, mainly the size of CTRZ and the distribution of tangential velocity.

Comparison of the predicted and measured velocity profiles

For comparison, the axial and tangential velocities predicted by the two turbulence models, together with the experimental results, are shown in Figs. 9 and 10 respectively. In the figures, H is a measuring position from the exit plane of the annular passage.

The experimental result of the axial component given by circles in Fig. 9 shows that there is a quite large central recirculation zone which extends up to H = 143 mm, and a small corner recirculation zone which vanishes soon after H = 26 mm, confirming existence of a strong swirling flow in the double-swirler com-

bustor, as predicted by the simulation. Meanwhile the experimental result of tangential component in Fig. 10 reveals the physical feature of a forced flow for the swirling flow, when H is greater than 46 mm.

The predicted axial velocity distributions show that in the region where the distance H from the exit of the double swirler is smaller than 46 mm, the predictions of both turbulence models are in good agreement with the experimental results, as can be seen from Fig. 9. As the distance increases, the standard κ-ε model continues showing good agreement, only underpredicting the length of recirculation zone slightly, compared to the experimental result. The RNG κ-ε model, however, overpredicts the width of the recirculation zone at distances greater than 56 mm, although the comparison with the experiment shows improvement as the distance H increases further. On the other hand, the predicted tangential velocity distributions in Fig. 10 show that the two models again give results which agree well with the experimental result at distances less than about 56 mm. With greater distances, however, the standard κ-ε model underpredicts the tangential velocity within certain radial distances, while the RNG κ-ε model still shows good agreement with the experiment data. It is known that the profile of tangential velocity component in the swirling flow can be considered as a combination of forced-vortex (rigid-body rotation) and free-vortex (potential-vortex) flows. The turbulent characteristics of the swirling flow between the forced-vortex and surrounding free-vortex regions are different. The comparisons above indicate that the RNG κ-ε model well predicts the characteristics of the forced motion in the swirling flow, while the standard κ-ε model fails to show this important physical feature.

One important transport property, the eddy viscosity μ_t, which is determined by the calculated values of κ and ε, as defined in the section 3, can greatly affect the diffusion coefficients in turbulent transport processes such as momentum, heat and mass transfers. Due to the modification of κ and ε transport equations, the κ and ε distributions in the calculation using the RNG κ-ε model have been changed, and the turbulent kinetic energy becomes relatively smaller near centerline than near the wall at the same section, as shown from the predicted results in Figures 11(a) and 11(b). The model thus decreases the turbulent viscosity μ_t in the forced-vortex region, increases the value in the free-vortex motion relatively, and results in an improved distribution of the tangential velocity. On the other hand, the RNG model still assumes that the turbulence in the flow is isotropic, the turbulent viscosity that gives the better distribution of tangential velocity is not appropriate for the momentum equation governing the axial velocity, and this is probably the reason for discrepancy between the CTRZ size predicted by the RNG model and the one measured from the experiment under the flow condition considered in this work.

Comparison of the predicted and measured fuel concentration distributions

Comparisons between the simulation and experimental results for the fuel distribution in the DS burner are presented in Fig. 12 for five different sections, where Ca represents the overall concentration. As can be seen, the predictions are in good agreement with the experimental data. The fuel concentration tends to spread very quickly in the radial direction with increasing the distance from the inlet and becomes almost uniform at 16 mm, indicating very good mixing as a result of swirling flow and the opposing flows in the combustor.

3.1.2 LS Burner (Case 8)

Standard κ-ε model

For the LS burner, the predicted results for Case 8 with the standard κ-ε model are presented in Figs. 13(a)-(e). As can be seen, both CTRZ and CRZ are formed, which gives the general flow pattern in burners. The strong swirling motion makes the flow reversed right after the inlet, as in Figs. 13(a)-(c). The fuel distribution in Fig. 13(d), which is characterized with two peaks, is determined by two factors, the injection angle (60 degrees in this case) and the swirling motion induced by the swirler. The flow also tends to be fully developed at the burner exit.

Comparison of the predicted and measured fuel concentration distribution

The available experimental data for conventional swirler (LS) are the fuel concentration distribution in the burner (Case 8). The comparison between the experiment and the predicted results (using the standard κ-ε model) is given in Fig. 14, where Ca refers to the overall fuel concentration. As can be seen, both calculation and experimental results show

good agreement. Due to the swirling motion, mixing is greatly enhanced in the burner, resulting in a uniform concentration distribution in a short distance. The fuel distributions obtained with the other two different turbulence models, e.g. the RNG κ-ε model and the Reynolds Stress Model, are also compared with the experimental data, and the comparisons are similar to that of the standard κ-ε model. This again confirms the similarity of flow fields in the front region predicted using the three different turbulence models.

3.1.3 SS Burner (Case 10)

Standard κ-ε model

Calculation is also performed for the SS burner to study the flow in the burner and the effect of swirler size (the hub diameter) on the flow. Figures 15(a)-(e) give the results for Case 10, which has the same inlet conditions as in Case 8. Compared with Fig. 13, it can be seen that while the general flow patterns and the fuel distributions are similar for the LS and SS burners, the different hub sizes do cause change of CTRZ size. As can be seen, when the hub is smaller (the SS swirler), the width of CTRZ is decreased at the front region, the two peaks in the fuel distribution approach closer to each other. The maximum values of tangential velocity near the burner inlet, also get closer, making the swirling effect increased and the reversed flow in that zone intensified. However, the change is not substantial in terms of the flow characteristics in the two conventional burners.

RNG κ-ε model and Reynolds Stress Model (RSM)

In addition to the standard κ-ε model, the RNG κ-ε model and the Reynolds Stress Model (RSM), are also used to study the effects of turbulence models on the predictions for the conventional burner. Figures 16 and 17 present the results predicted with the other two turbulence models for Case 10. As can be seen from the vector velocity and stream function plots, all the results show the general characteristics of strongly swirling flows, e.g, the existence of CTRZ and accompaning CRZ. In addition, the fuel distributions predicted with three different turbulence models are nearly the same. The three models, however, do give different prediction results in terms of the size of CTRZ. Figures 18(a)-(d) show comparisons of the calculated axial velocity, tangential velocity, turbulent kinetic energy as well as turbulent dissipation rate distributions with the three models, and it can be seen that the RSM predicts the longest CTRZ, followed by the RNG κ-ε model, although the three models gives close results for the width of CTRZ in the front region of the burner.

The most remarkable difference occurs in the tangential velocity distribution. As shown in Fig.18(b), the RNG κ-ε again shows improvement in prediction of the combined free and forced vortex motion in the strongly swirling flows, as in the case for the DS burner, and the RSM also well captures the important feature. While the improvement in the RNG κ-ε model is due to the modification of κ and ε transport equations or the turbulent viscosity μ_t, as discussed above, the mechanism for the improved prediction of vortex motion in the RSM is completely different, it is attributed to the duplication of the characteristics associated with anisotropy and curvature in swirling flow. Currently, there exist actually two separate viewpoints in calculation of strongly swirling flows. The first one assumes that the anisotropic eddy viscosity and the RNG Boussinesq hyposesis adequately describe the stress distributions and the source of predictive error is a consequences of the modeled term in the κ-ε equations, therefore only the modifications to the κ and ε equations are needed. The second one, however, proposes that the eddy viscosity approach is inherently inadequate, and that a redistribution of stress magnitudes is necessary, so a higher-order closure such as the RSM is needed. The calculation results in the present work show that, while both RNG κ-ε model and the RSM could improve the tangential velocity distribution in terms of prediction of free and forced vortex motions, the RSM seems to be able to reproduce the motion better. However, it is not known if the RSM could produce good prediction of CTRZ size, because the measurements of the velocities in the conventional burner have not been conducted. Besides the confirmation of the existing problems mentioned in section 1, the present calculations also find the importance of inlet conditions for stress components in using the RSM, but its specification is obviously difficult without accurate experimental data. It seems, therefore, that further research work, both development and verification of turbulence models, is needed for solution of strongly swirling turbulent flows, in order to solve the on-going argument in this field.

3.2 Effects of Inlet Conditions on Flows in the buners

The predicted results for the DS and conventional burners under different inlet conditions will be given in the following. The inlet conditions here include different inlet values for both fuel and air streams, as summarized in Table 1. In addition, all the results given below are obtained using the standard κ-ε model, based on the fact that different turbulence models all gives similar flow patterns, particularly in the front region of the burners, as disscused in the last section.

Figure 19 shows the predicted results for Case 2, where the air flow rate is increased twice as much as that of Case 1, and $M_2 = 2M_1$ is retained. It can been seen that the flow characteristics and distributions are quite similar to the results in Fig. 6.

Figure 20 is the predicted results for Case 3, where the total air flow rate is kept the same as Case 2, but the air mass flow rate ratio between the two swirlers is set to be $M_1 = 2M_2$. From Figs. 20(a) and (e), it can be seen that the flow pattern in the burner has been greatly changed. The increased flow rate coming from the inner swirler increased the jet velocity at the double swirler exit, making the jet velocity there even higher. The high-speed jet in turn affects the downstream flow significantly. As can been seen in Figs. 20(b) and (d), it makes the CTRZ smaller and more narrow and changes the fuel distribution in the flow. The tangential velocity distribution in Fig. 19(c) is also quite different from that of Case 2, due to increased swirl in the first swirler.

Cases 4-6 are designed for the study of the effects of the variation of fuel injection velocity on the flow field, in which both the total air mass flow rate and ratio of air flow rate remain the same ($M_1 = M_2$), but the fuel flow rates (hence the injection speed) in Case 5 and Case 6 are set to be two and four times of that in Case 4 respectively. The results for Cases 4, 5 and 6 are respectively given in Figs. 21, 22 and 23. It can be seen that, while the distributions of velocity vector, axial velocity, tangential velocity, fuel concentration and stream function in Fig. 21 are similar to those in Fig. 19, the increase of the fuel injection velocity in Case 5 significantly changes the flow pattern as well as the fuel distribution given in the flow, although the tangential velocity distribution is somewhat different in Fig. 22. The change is more obvious when the fuel injection velocity is further increased, as shown in Fig. 23.

Case 7 keeps the high fuel injection velocity and the ratio $M_1 = M_2$, as that in Case 5, but the air mass flow rate is set to be higher, the air velocity in both swirlers are thus increased. The predicted results are given in Fig. 24. Interestingly, all the distributions are changed from Fig. 22 (Case 5) back to the ones similar to Fig. 21 (Case 4). Combined with the results given above, Case 7 reveals significant effect of the inlet conditions of the second swirler on the flow.

Figures 25(a)-(e) are predicted results for Case 9 (the LS swirler), where the fuel mass flow rate is the same as in Case 8, but the incoming air flow rate, hence the inlet velocity, is increased. From Fig. 25, it can be found that the sizes of CTRZ and CRZ are nearly the same as those in Fig. 13, and the velocity (both axial and tangential) is increased proportionally, which makes the flow pattern almost the same.

The fact that the flow pattern in the conventional burners with a fixed vane angle swirler is affected little by the inlet conditions makes it different from the DS burner. As can be seen from the discussion above, the flow features in the DS burner can be controlled aerodynamically by the inlet flows, and the high velocity jet which is produced by the double swirler makes the mixing process intensified due to opposing effect of the jet and reverse flow in the burner. Consequently the improved mixing process between air and fuel is helpful in reducing the NO_x emissions when the combustion occurs.

4. Conclusions

From the present study, the following conclusions can be drawn:

(1) The standard κ-ε model, RNG κ-ε model and RSM can all predict the general flow features of the strong swirling flows considered in this work. The predicted results using the different models, however, show different details of flow characteristics. They predict different CTRZ sizes, mainly in the downstream of the flow. The experimental evaluation conducted for the flow in the DS burner indicates that the predicted CTRZ sizes given by the standard κ-ε model show comparatively good agreement with the experiment data, while the RNG κ-ε model is shown to be able to improve the prediction of the rigid vortex motion

in the strongly swirling flow. The RSM model is also found to be able to improve the prediction of the motion. The complete assessment of the different models, however, depends on further accurate measurements of the flow field and stress components in the swirling flow.

(2) Comparisons between predictions and experimental data for the fuel distribution show good agreement. The fact that the fuel distributions obtained with different turbulence models are quite close in the front region of the burners confirms the similarity of the predicted flow field in the same region.

(3) Flows in the three burners, including the DS and LS, SS burners, are all characterized with strongly swirling flow patterns, e.g. the existence of an large central toroidal recirculation zone and an accompaning corner recirculation zone.

(4) The study of the effects of inlet conditions on flow patterns discovers that the double swirler possesses unique advantages over conventional swirlers, e.g., the flow pattern as well as the fuel concentration distribution in the burner could actually be controlled by changing the ratio of air flow rate in the inner and outer swirlers or the fuel flow rate in the fuel nozzle. A high velocity jet is produced near the exit of the double swirler, and it may enhance the mixing process of the air and fuel due to opposing effect of the jet and reverse flow in the burner.

(5) The flow patterns in the two conventional burners, LS and SS, are similar, and they do not change significantly with the variation of inlet conditions when the swirler vane angle remains the same. The difference in the swirler hub size, however, changes the size of CTRZ, and the smaller hub may decrease the width of CTRZ in the burner.

Acknowledgments

The authors wish to thank Mr.Takashi Terasaki, who was a research fellow at NAL in the period 1992-1994, for providing the experiment data used in this paper.

References

[1] S. Hayashi, Compatibility between Low-NOx Emissions and High-Combustion Efficiency by Lean Direct Injection Combustion, ASME 95-GT-276, 1995.

[2] T. Terasaki and S. Hayashi, Lean Non-Premixed Combustion for Low-NOx Gas Turbine Combustor, Proceedings of the 1995 Yokohama International Gas Turbine Congress (II), pp. 353-358, 1995.

[3] N. Syred and J.M. Beer, Combustion in Swirling Flows: A Review, Combustion and Flame, vol. 23, pp. 143-201, 1974.

[4] A.K. Gupta, D.C. Lilley, and N. Syred, Swirl Flow, Abaacs Press, Tunbridge Wells, England, 1984.

[5] D.G. Sloan, P.J. Smith and L.D. Smoot, Modeling of Swirl in Turbulent Flow System, Progress in Energy and Combustion Science, vol. 12, pp. 163-250, 1986.

[6] M. Nallasamy, Turbulence Models and Their Applications to the Prediction of Internal flows: A Review, Computational Fluids, vol. 3, pp. 151-194,1987.

[7] G.J. Sturgess and S.A. Syred, Calculation of Confined swirling Flows, International Journal of Turbo Jet Engines, vol. 7, pp. 103-121, 1990.

[8] P. Koutmos and J.J. McGuirk, Isothermal Modeling of Gas Turbine Combustors: Computational Study, Journal of Propulsion Power, vol. 7, pp. 1064-1091, 1991.

[9] P. Bradshaw, Effects of Stream Curvature on Turbulent Flows, AGARDogragh. Report No. 169, 1973.

[10] J.M. Khodadadi and N.S. Vlachos, Effects of Turbulence Model Constants on Computation of Confined swirling Flows, AIAA Journal, vol. 28, pp. 750-752, 1990.

[11] V. Yakhot and Orszag, S.A, Renormalization Group Analysis of Turbulence. I. Basic Theory, J. Scientific Comp., vol. 1, No. 3 1986.

[12] S. Fu, P.G. Huang, B.E. Launder and M.A. Leschziner, A Comparison of Algebraic and Differential Second-Moment Closures for Axisymmetric Turbulent Shear Flows with and without Swirl, Journal of Fluids Engineering, Transactions of ASME, vol. 110, pp. 216-221, 1988.

[13] M. Nikjooy and H.C. Mognia. A Second-Order Modeling Study of Confined Swirling Flow, International Journal of Heat Fluid Flow, vol. 12, pp. 12-19, 1991.

[14] W.P. Jones and A. Pascau, Calculation of Confined Swirling Flows with a Second Moment Closure, Journal of Fluids Engineering, Transactions of ASME, vol. 111, pp. 248-255, 1989.

[15] S. Hogg and M.A. Leschziner, Computation of Highly Swirling Confined Flow with a Reynolds Stress Turbulence Model, AIAA Journal, vol. 27, pp 57-63, 1989.

[16] J.M. Beer and N.A. Chigier, Combustion Aero-Dynamics, Applied Science, London, 1972.

[17] B.E. Launder and D.B. Spalding, The Numerical Computation of Turbulent Flows, Computational Methods in Applied Mechanics Engineering, vol. 3, pp. 269-289, 1974.

[18] C.M. Rhie and W.L. Chow, Numerical Study of the Turbulent Flow Past an Airfoil with Trailing Edge Separation, AIAA Journal, vol. 21, No. 11, pp. 1525-1532, 1983.

[19] S.V. Patankar, Numerical Heat Transfer and Fluid Flow, Hemisphere, New York, 1980.

[20] J.F. Thompson, F.C. Thames and C.W. Mastin, Boundary Fitted Curvilinear Coordinate System for Solution of Partial Differential Equations of Fields Containing any Number of Arbitrary Two-Dimensional Bodies, Report GR-2729, NASA Langley Research Center, 1976.

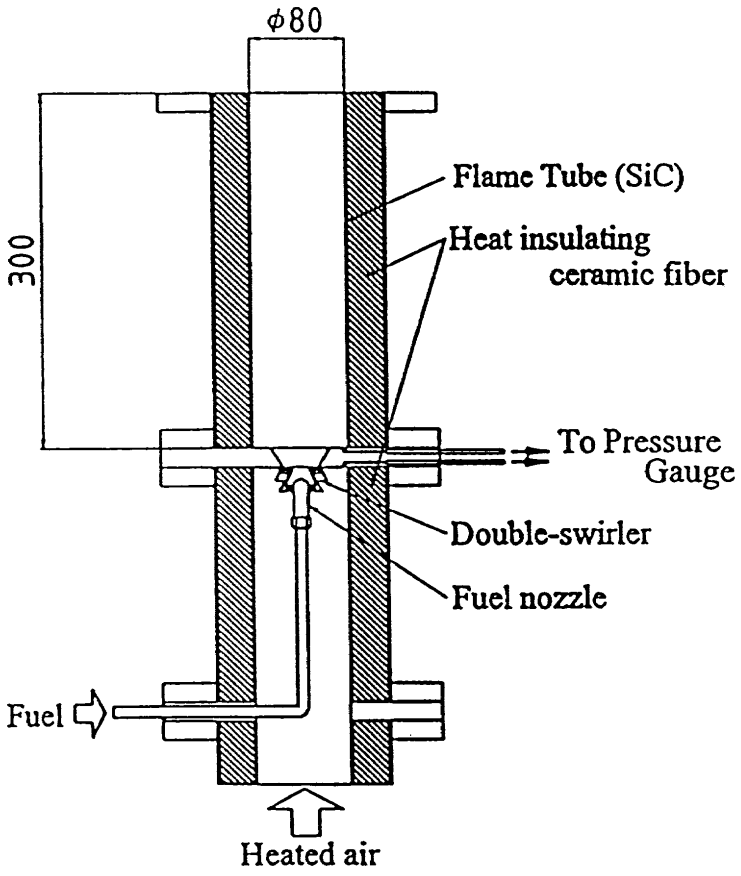

Fig. 1 Schematic diagram of flow system

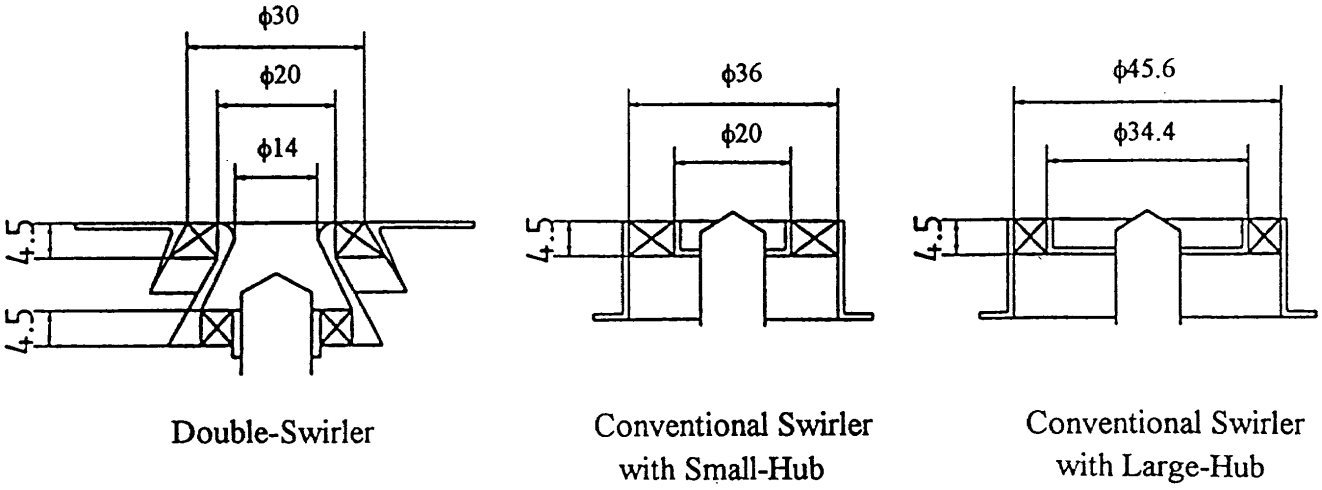

Fig. 2 Differential swiler configurations used in the burner

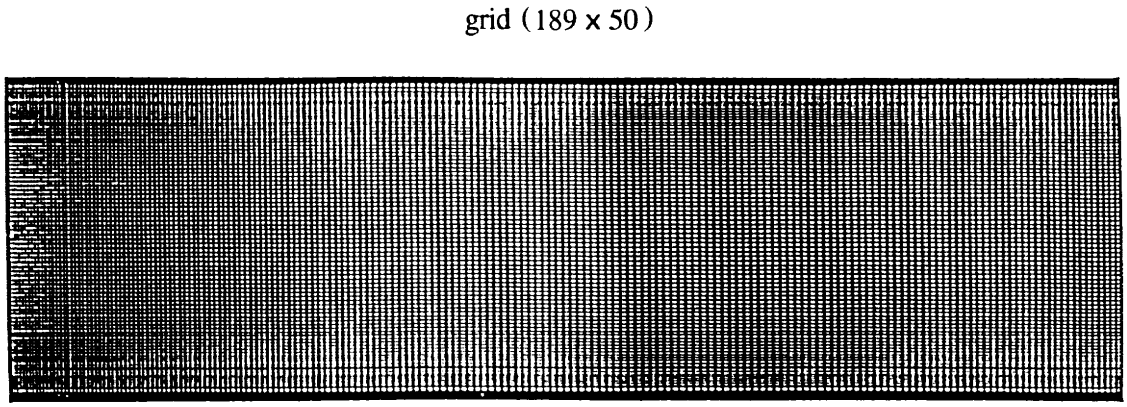

Fig. 3 The grid system for the conventional burners

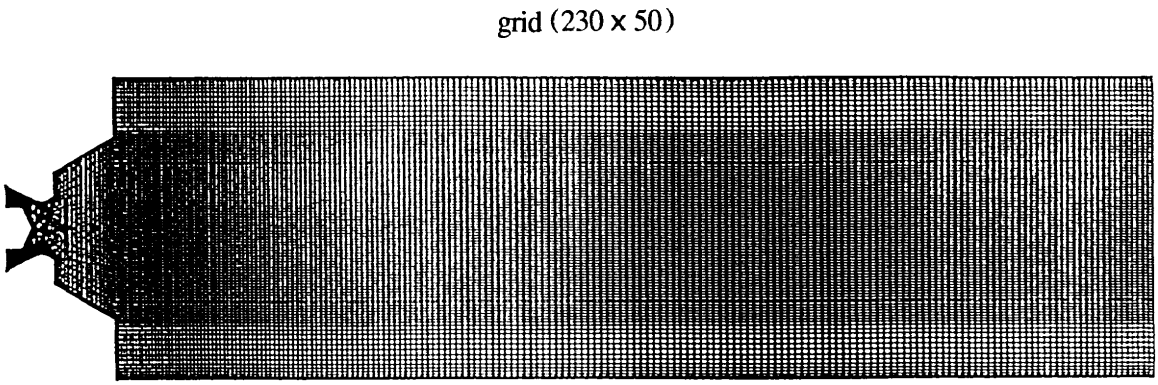

Fig. 4 The grid system for the DS burners

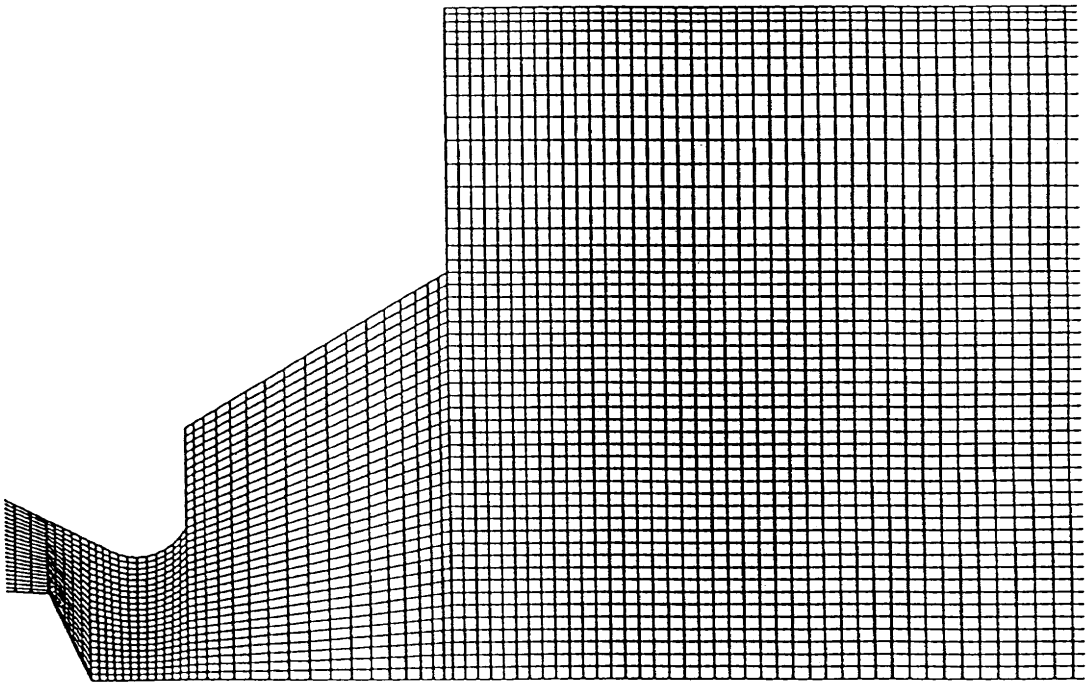

Fig. 5 The grid system in the double swirler

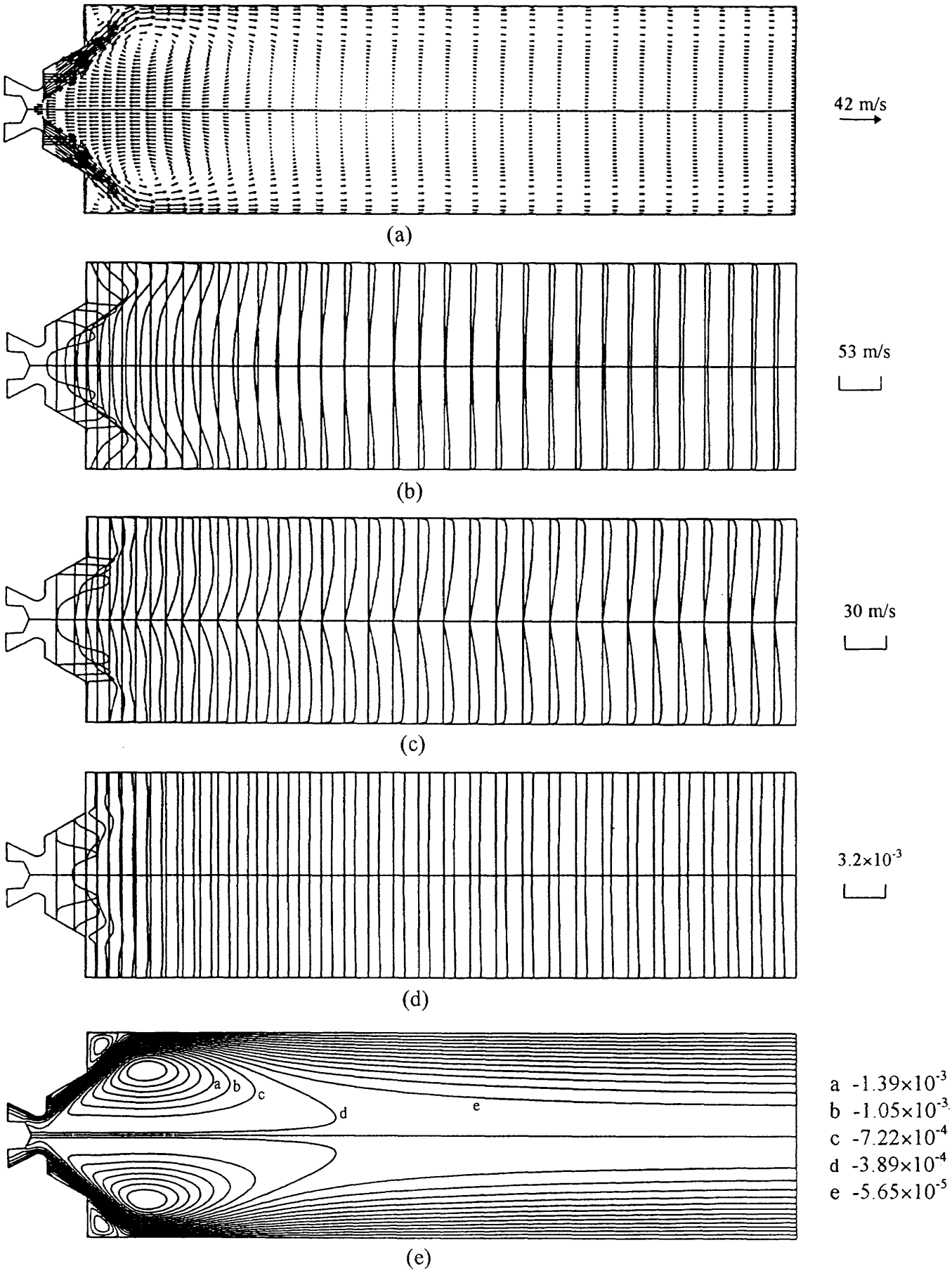

Fig. 6 Predicted results with the standard κ-ε model for Case 1 (a) velocity vectors, (b) axial velocity, (c) tangential velocity, (d) fuel concentration, (e) stream functions

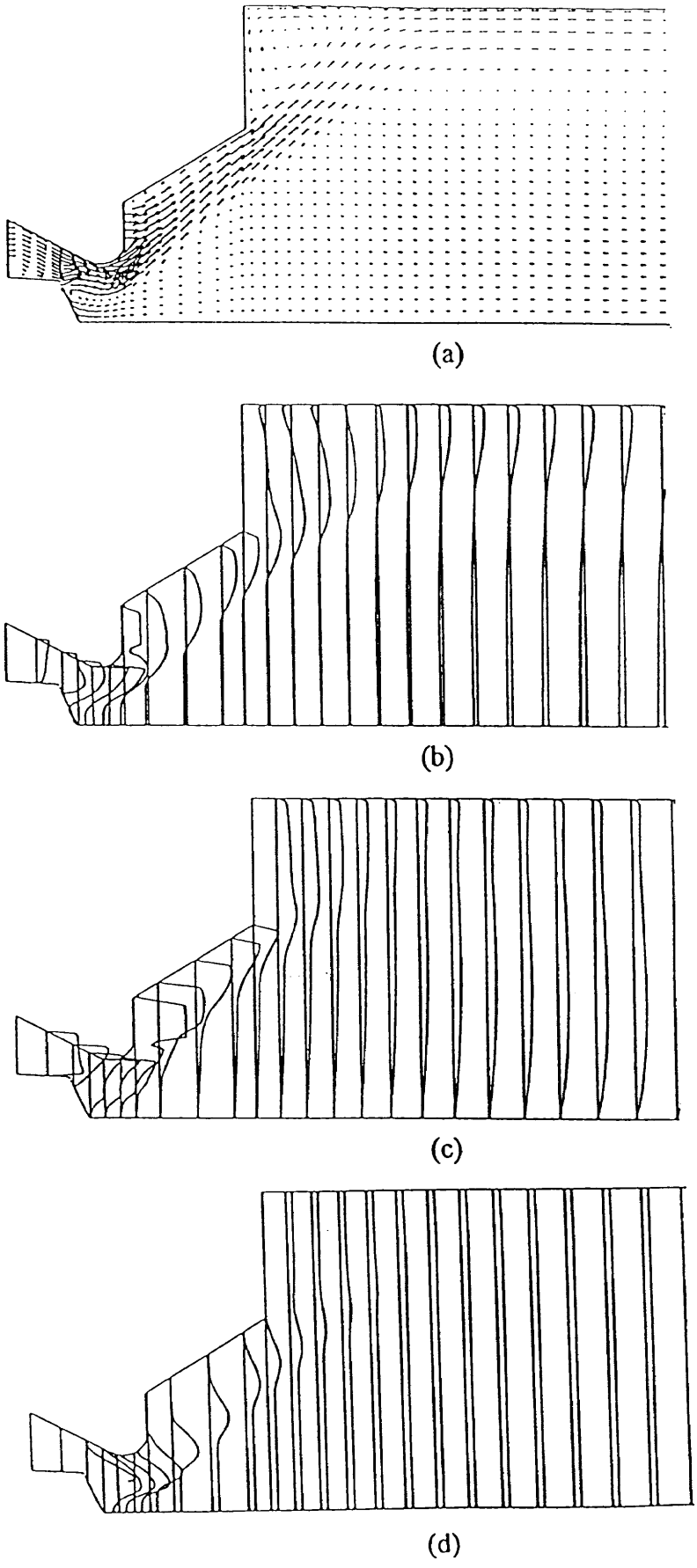

Fig. 7 Enlargement of parameter distributions in the double-swirler given by Fig. 6
(a) velocity vectors, (b) axial velocity, (c) tangential velocity, (d) fuel concentration

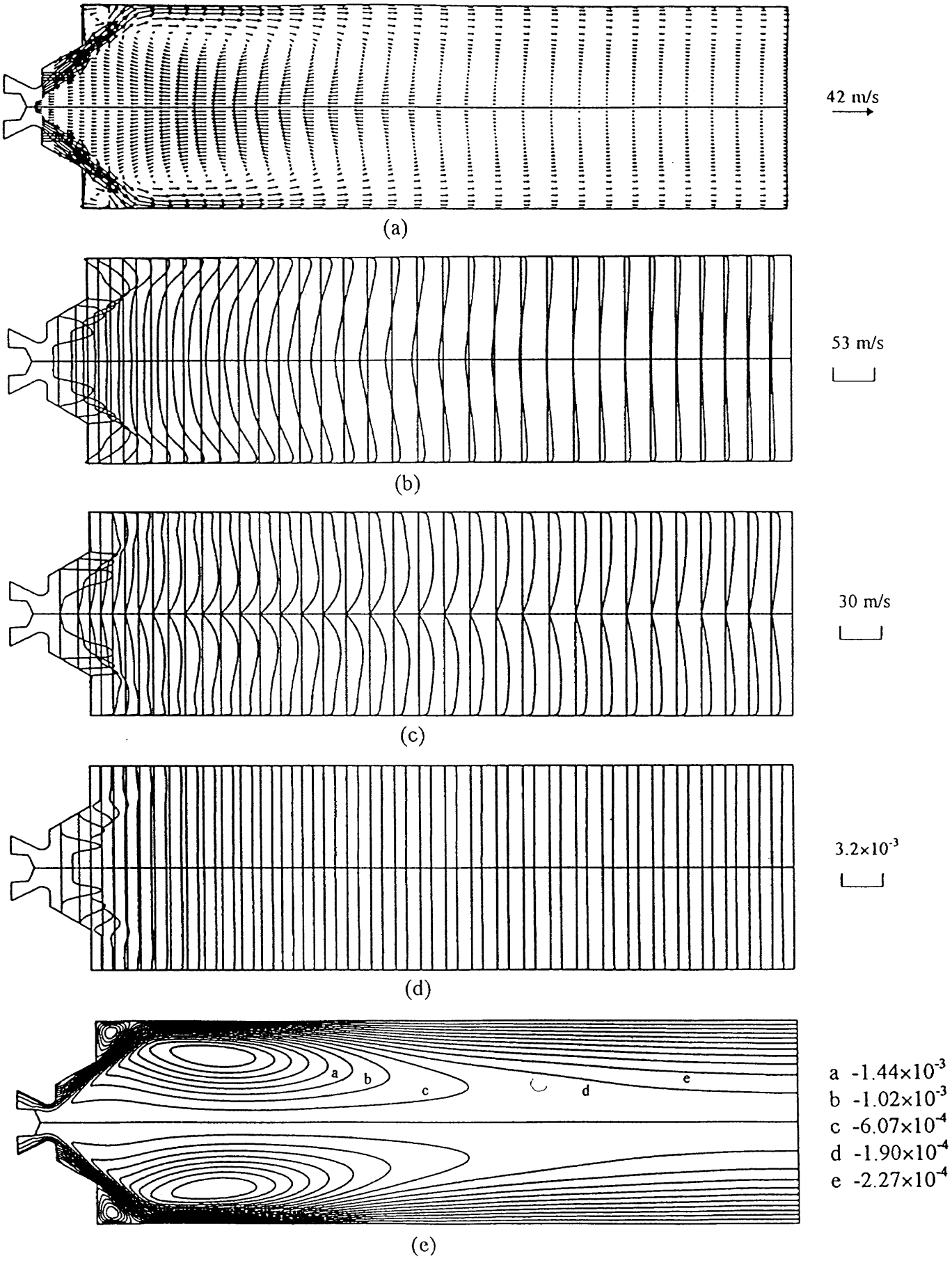

Fig. 8 Predicted results with the RNG κ-ε model for Case 1 (a) velocity vectors, (b) axial velocity, (c) tangential velocity, (d) fuel concentration, (e) stream functions

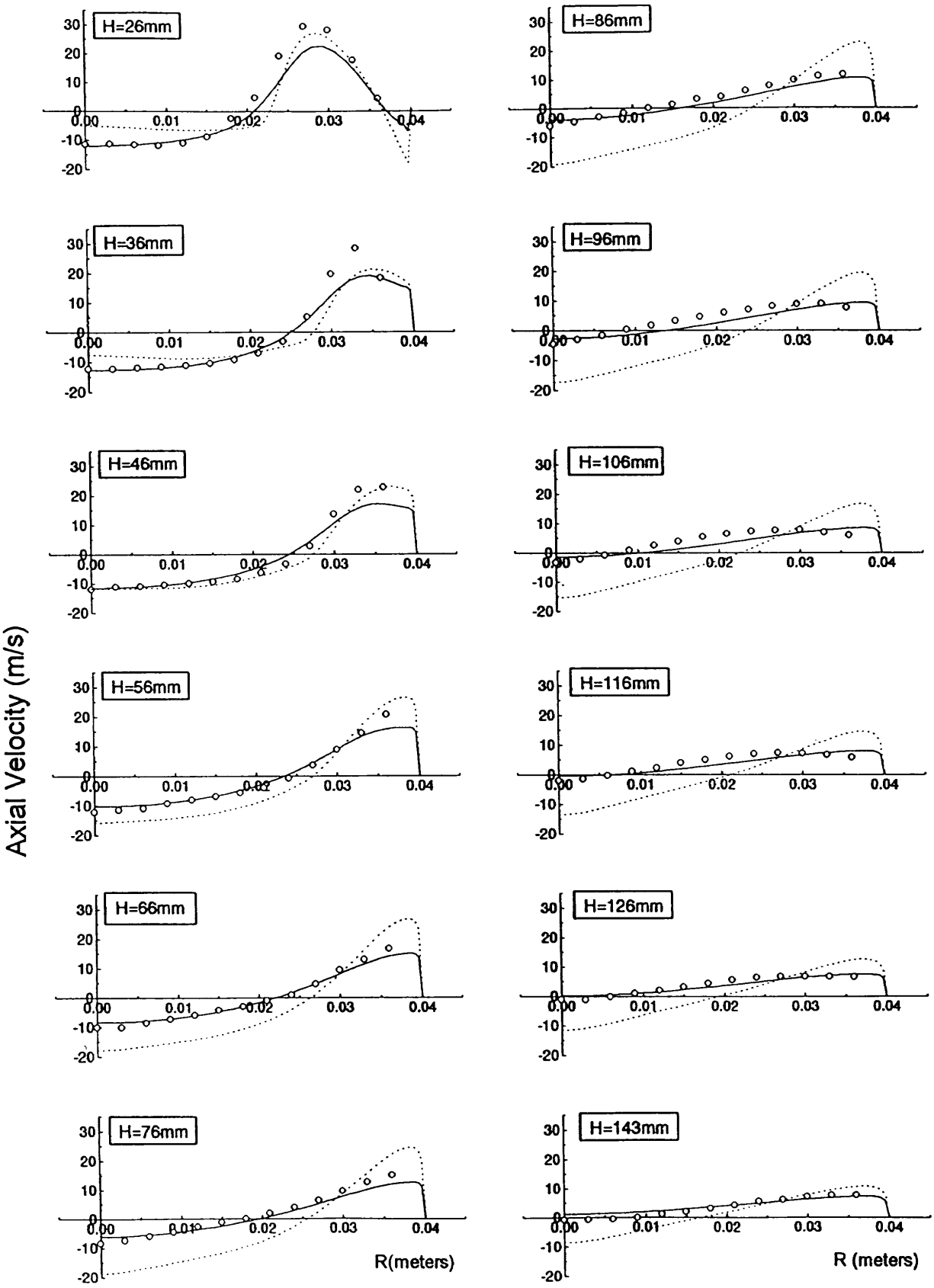

Fig. 9 Comparisons of prediction and experiment data for axial velocity distribution
(— κ-ε model - - - RNG κ-ε model ∘ experiment)

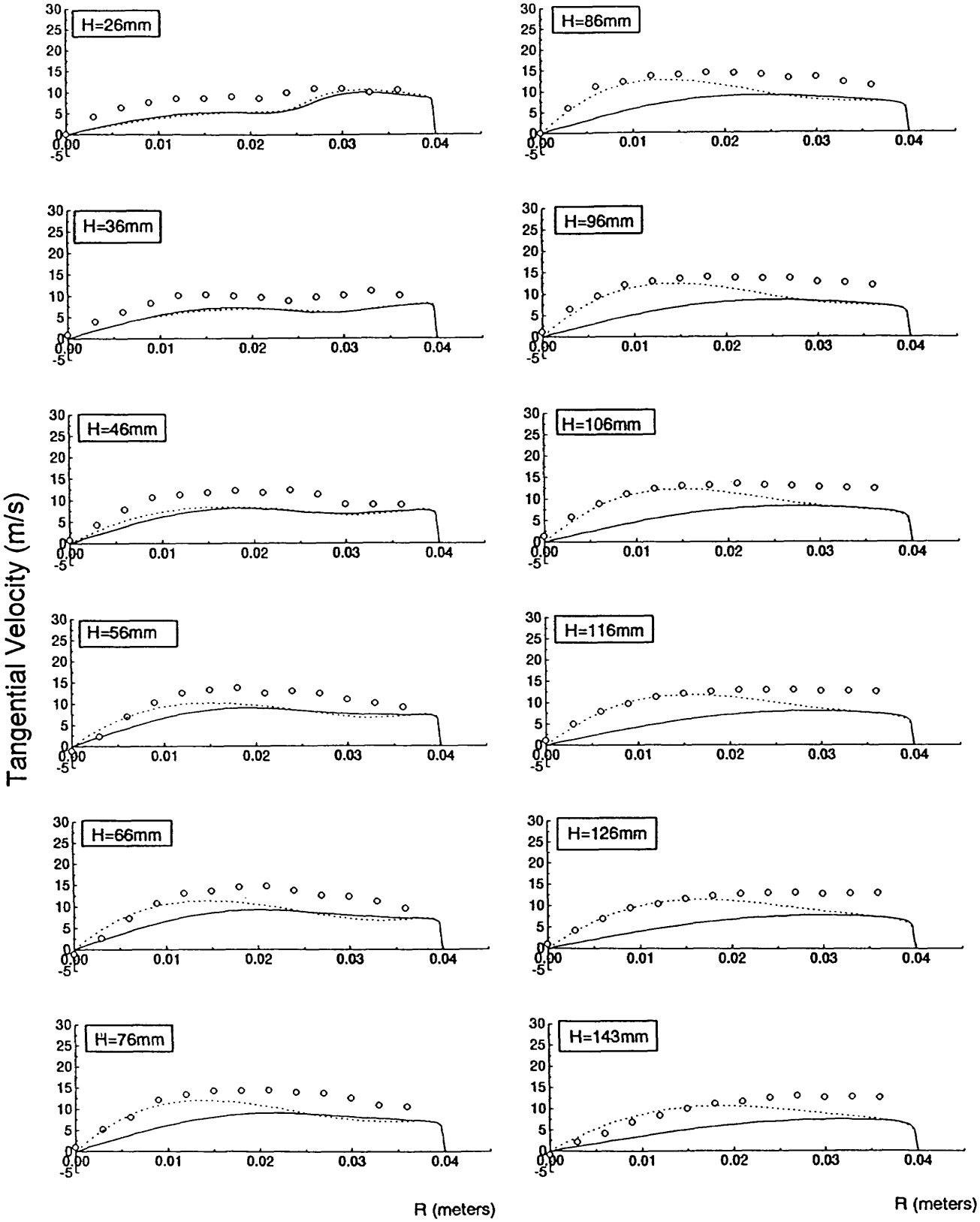

Fig. 10 Comparisons of prediction and experiment data for tangential velocity distribution (— κ-ε model - - - RNG κ-ε model ∘ experiment)

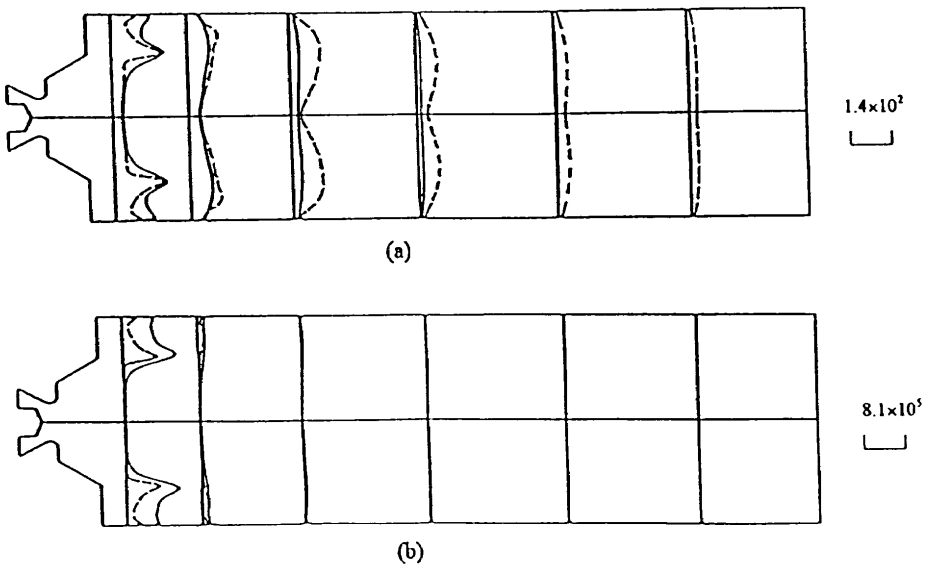

Fig. 11 Comparisons of predicted results obtained with different turbulent models
(a) turbulent kinetic energy (b) turbulent dissipation rate (— κ-ε model - - - RNG κ-ε model)

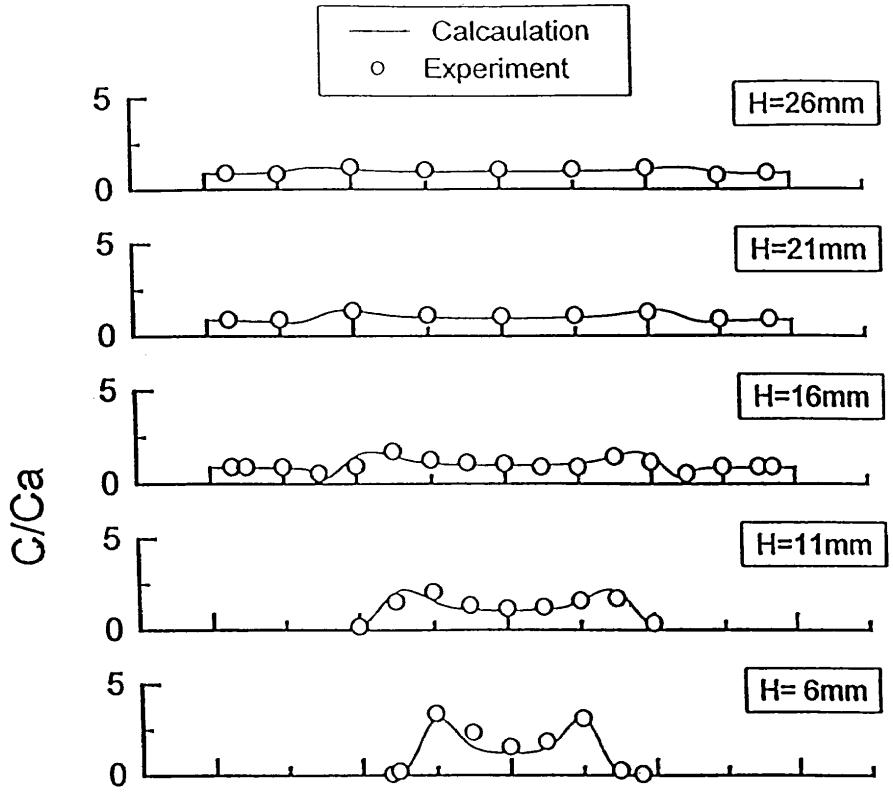

Fig. 12 Comparisons of prediction and experiment data for fuel concentration distribution (κ-ε model)

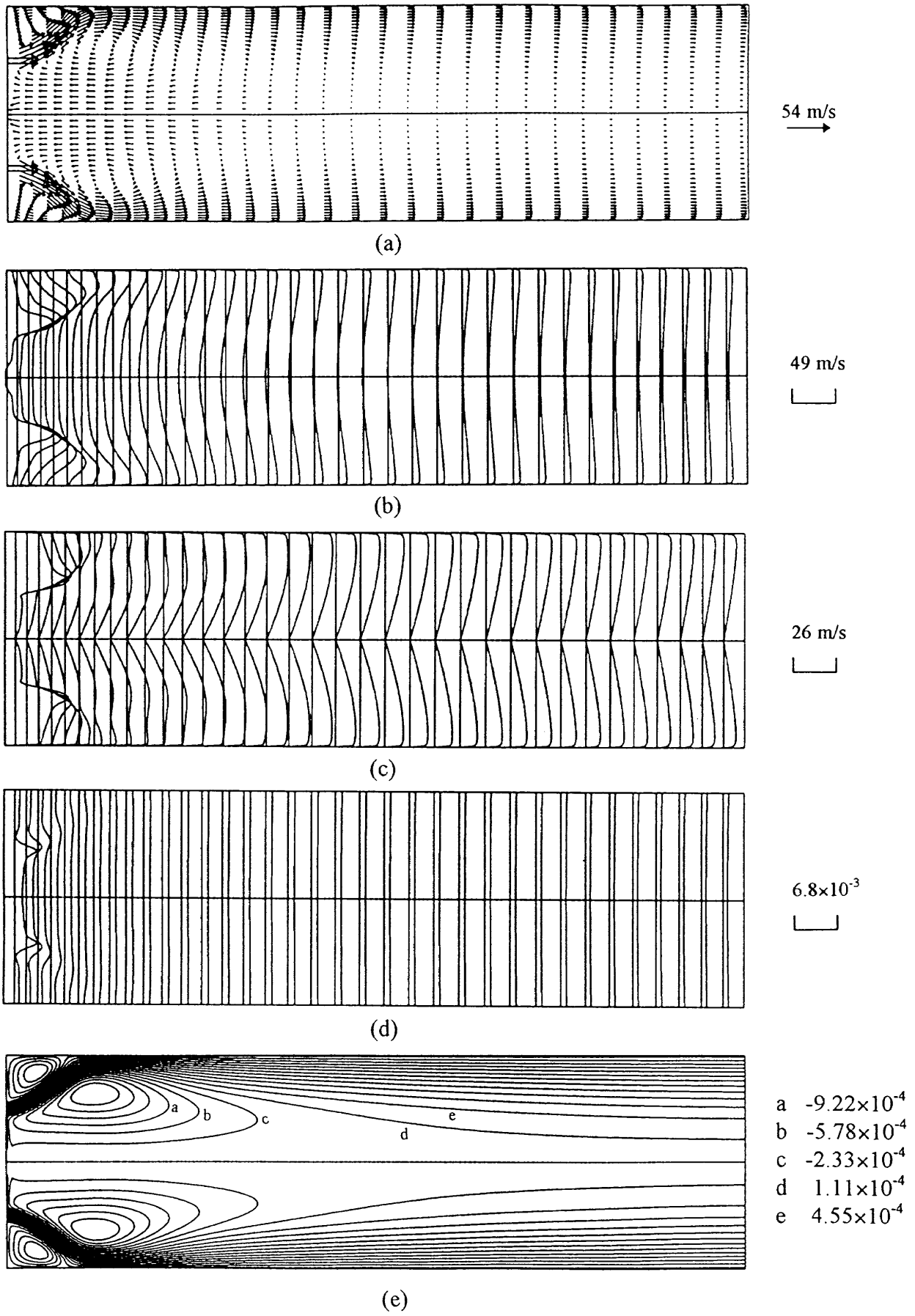

Fig. 13 Predicted results with the standard κ-ε model for Case 8 (a) velocity vectors, (b) axial velocity, (c) tangential velocity, (d) fuel concentration, (e) stream functions

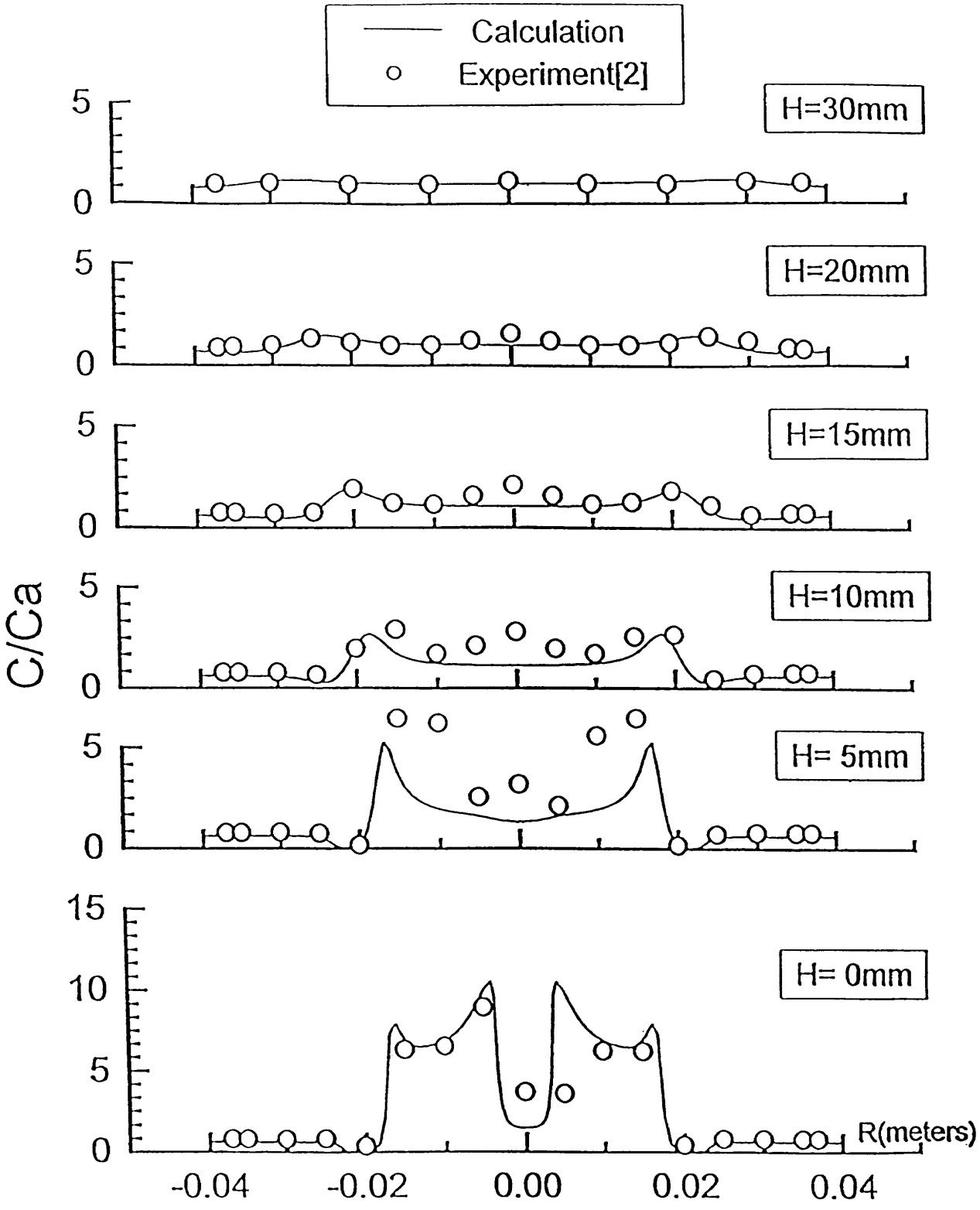

Fig. 14 Comparison of predictions and experiment data for fuel concentration distribution (Case 8)

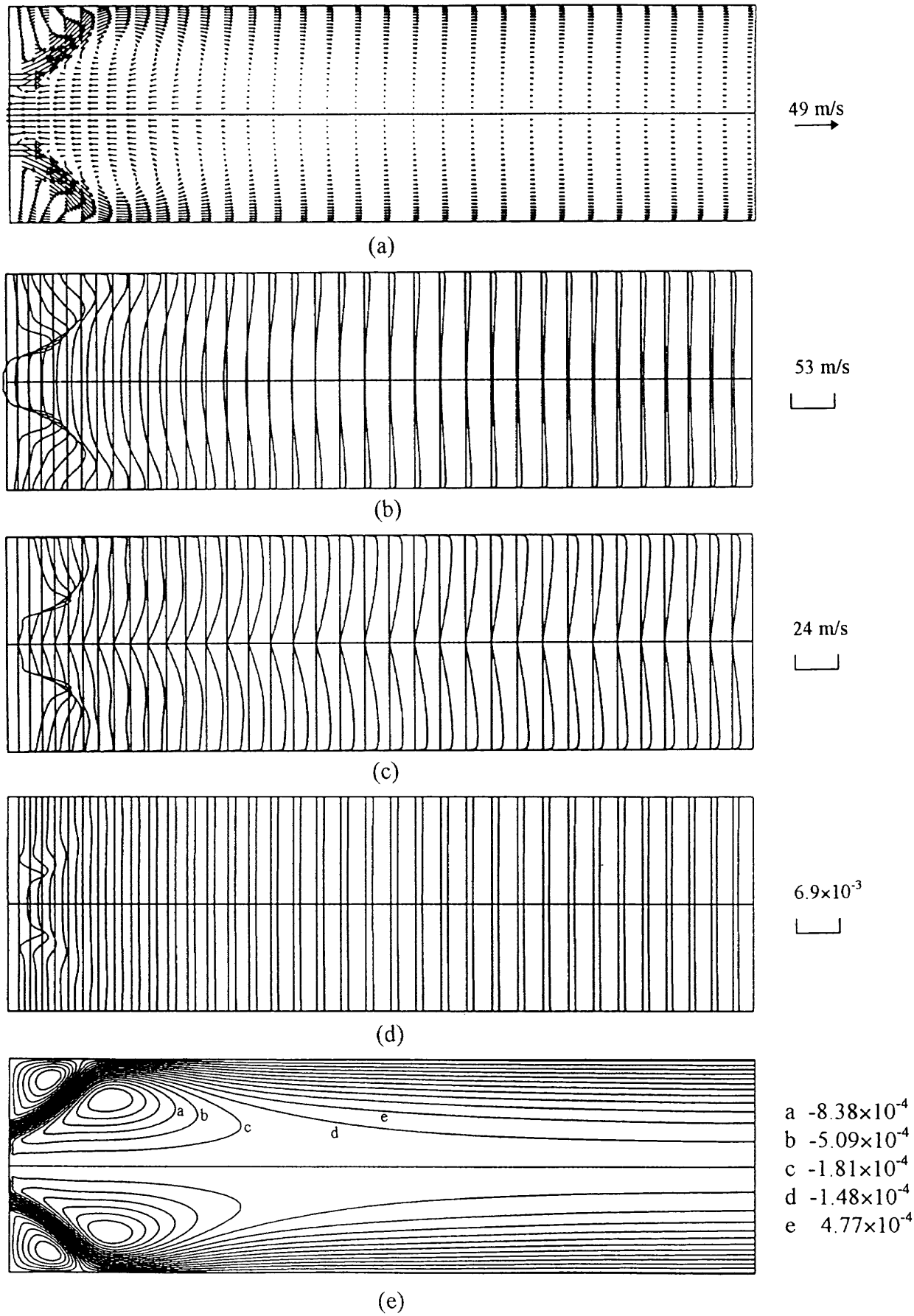

Fig. 15 Predicted results with the standard κ-ε model for Case 10 (a) velocity vectors, (b) axial velocity, (c) tangential velocity, (d) fuel concentration, (e) stream functions

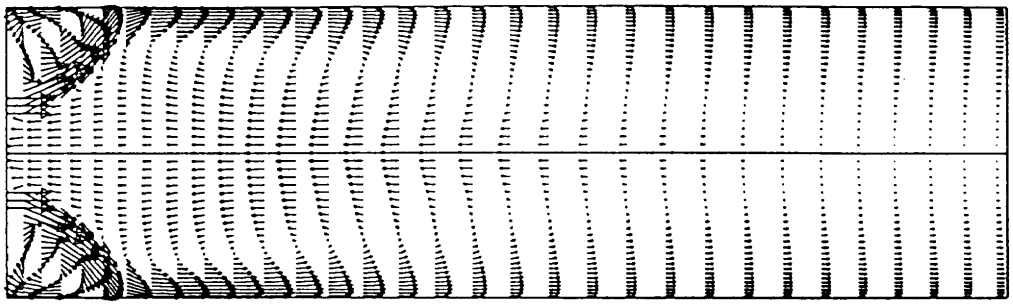

(a)

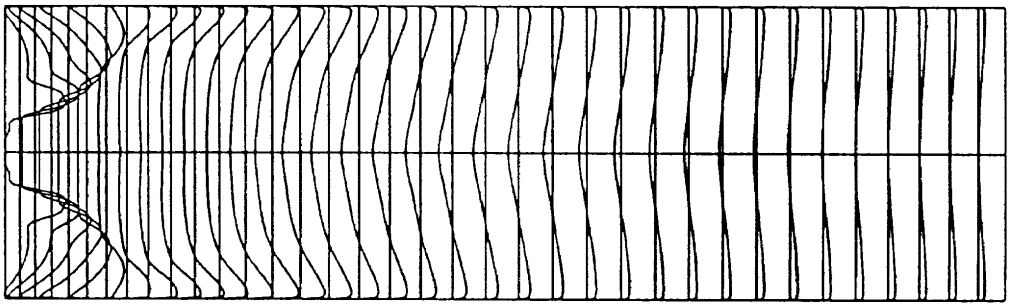

(b)

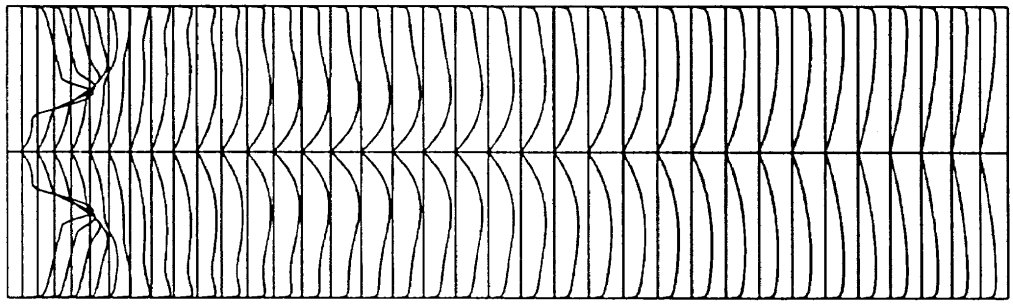

(c)

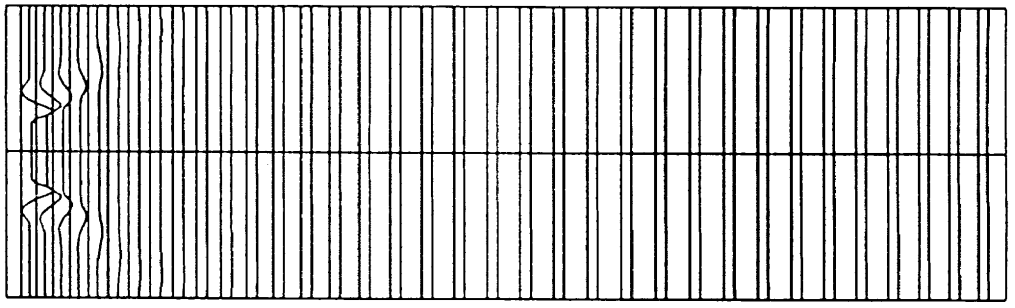

(d)

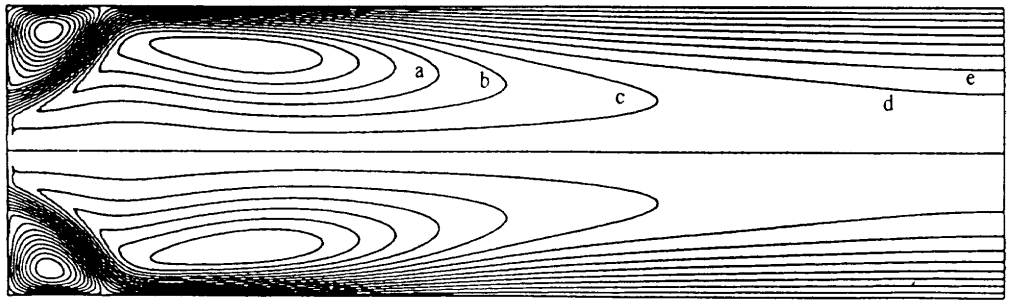

(e)

Fig. 16 Predicted results with the RNG κ-ε model for Case 10 (a) velocity vectors, (b) axial velocity, (c) tangential velocity, (d) fuel concentration, (e) stream functions

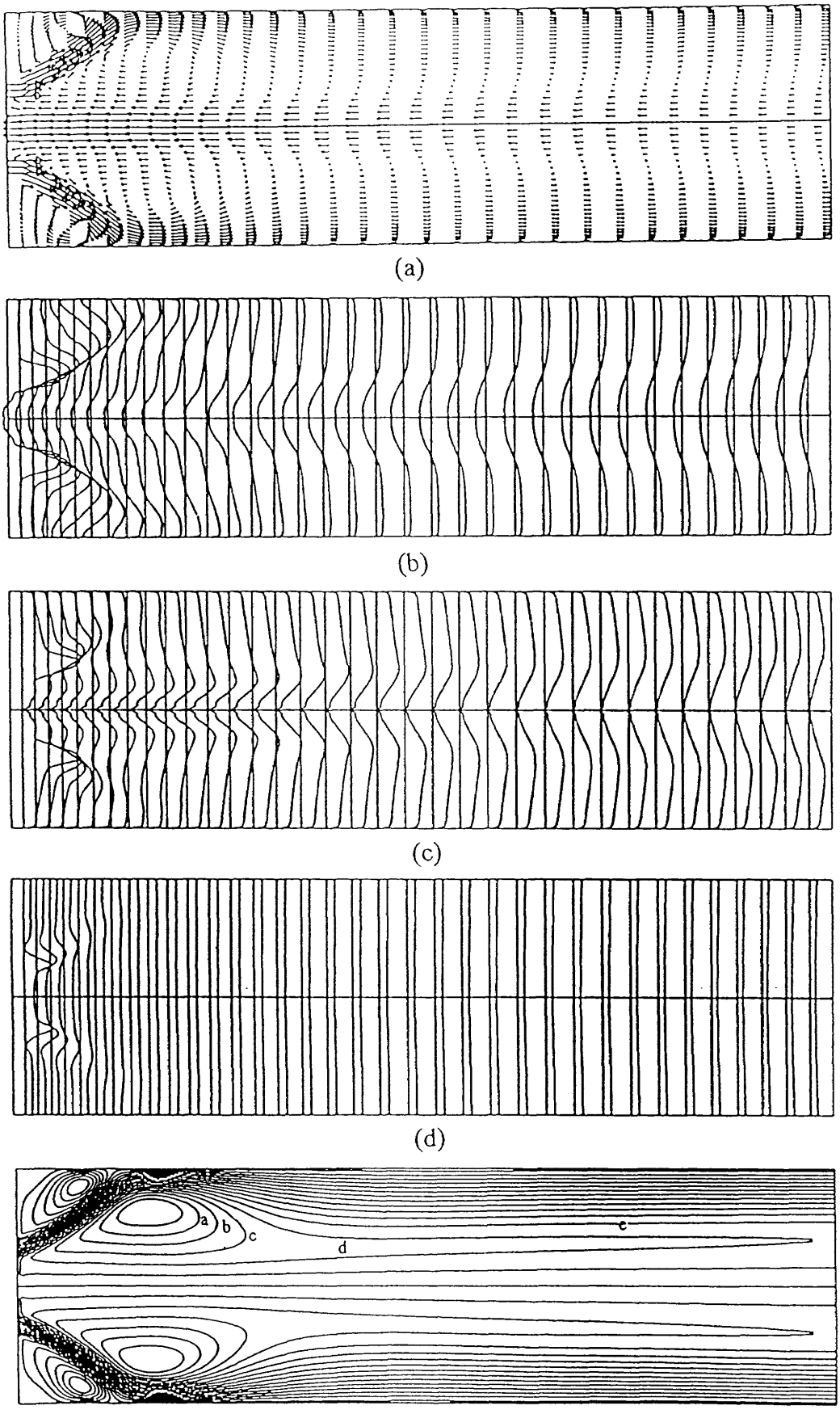

Fig. 17 Predicted results with the RSM for Case 10 (a) velocity vectors, (b) axial velocity, (c) tangential velocity, (d) fuel concentration, (e) stream functions

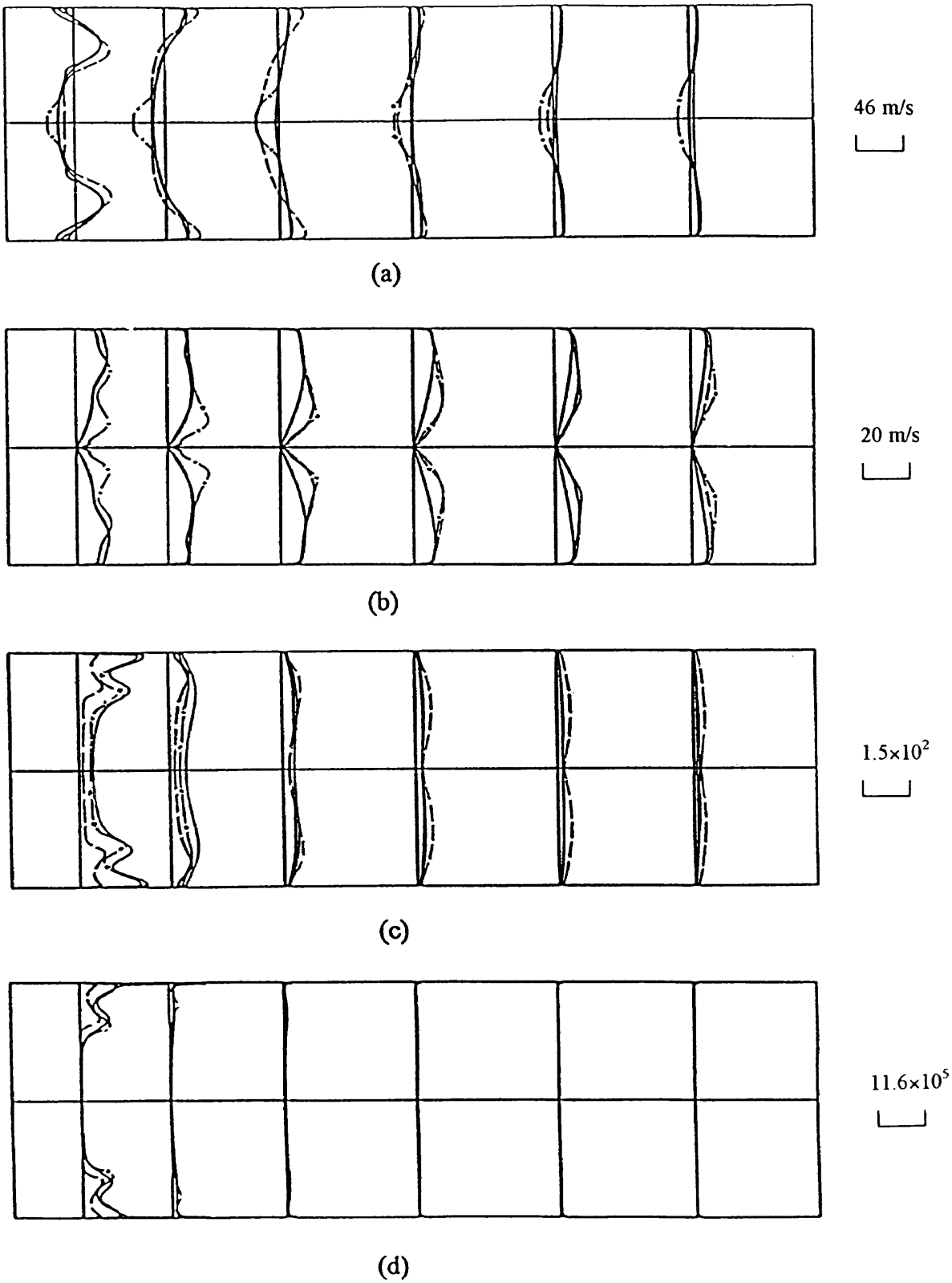

Fig. 18 Comparisons of predictions obtained with different turbulent models
(a) axial velocity (b) tangential velocity (c) turbulent kinetic energy
(d) turbulent dissipation rate (— κ-ε model - - - RNG κ-ε model ·-·-· RSM)

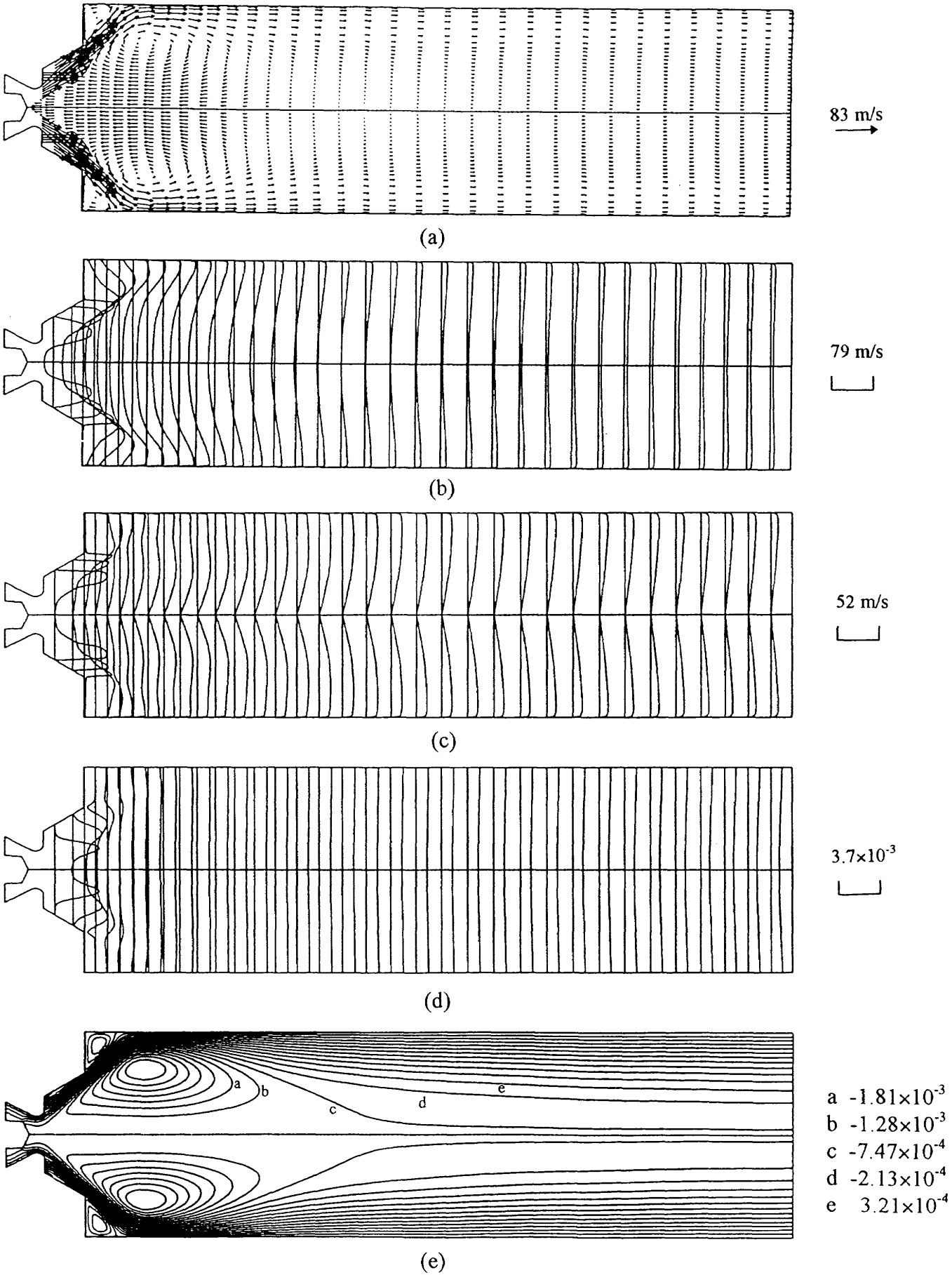

Fig. 19 Predicted results with the standard κ-ε model for Case 2 (a) velocity vectors, (b) axial velocity, (c) tangential velocity, (d) fuel concentration, (e) stream functions

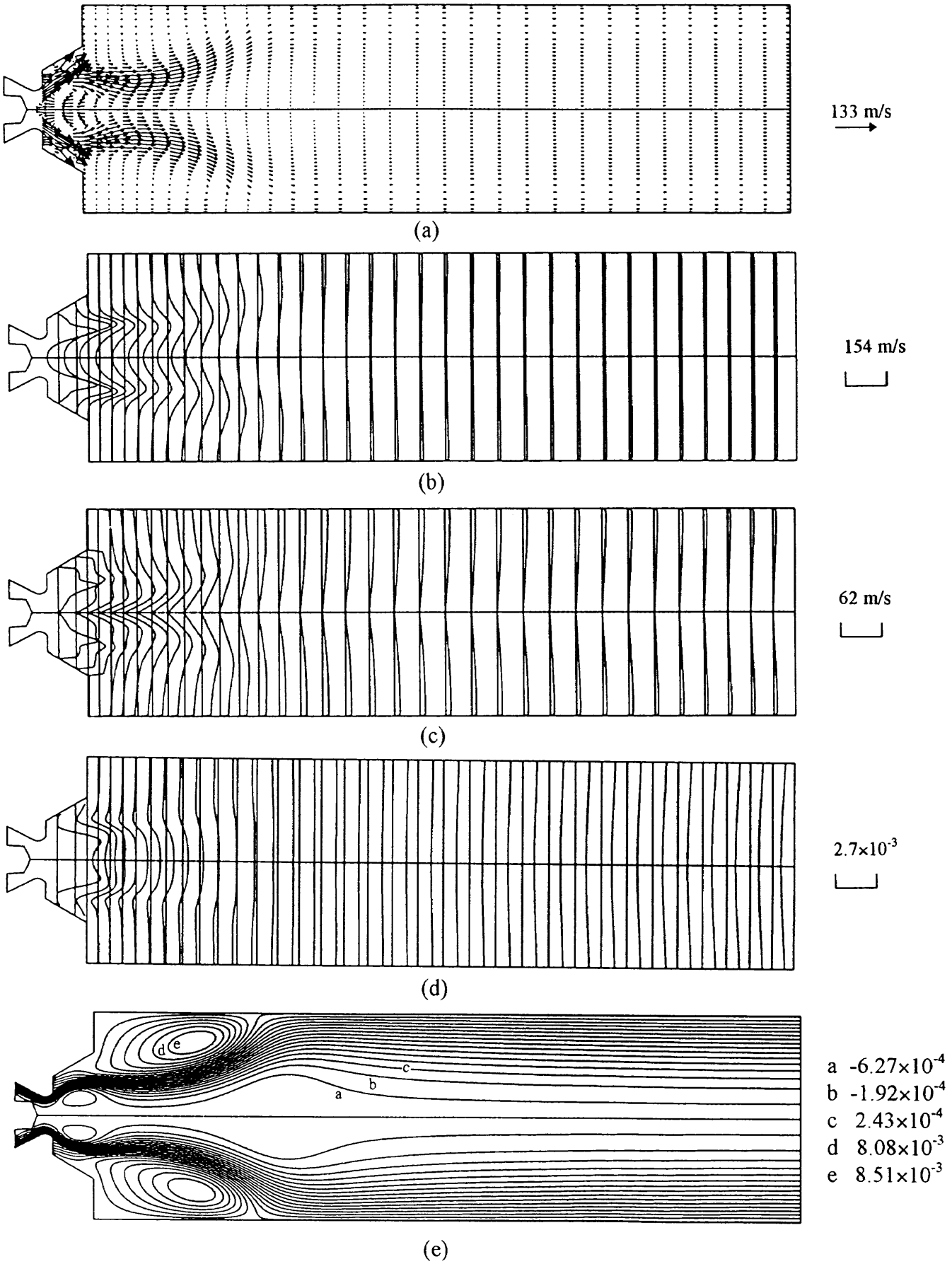

Fig. 20 Predicted results with the standard κ-ε model for Case 3 (a) velocity vectors, (b) axial velocity, (c) tangential velocity, (d) fuel concentration, (e) stream functions

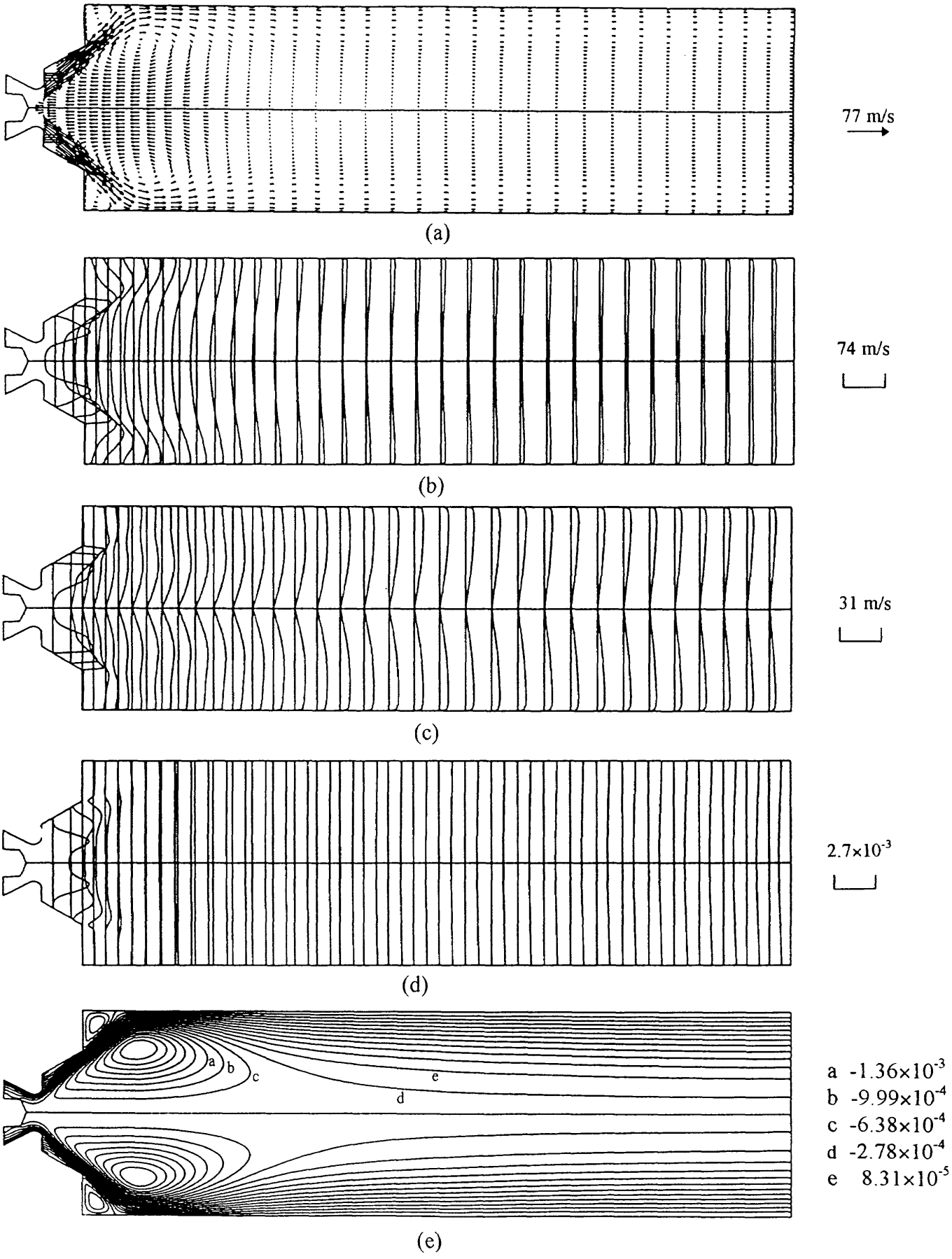

Fig. 21 Predicted results with the standard κ-ε model for Case 4 (a) velocity vectors, (b) axial velocity, (c) tangential velocity, (d) fuel concentration, (e) stream functions

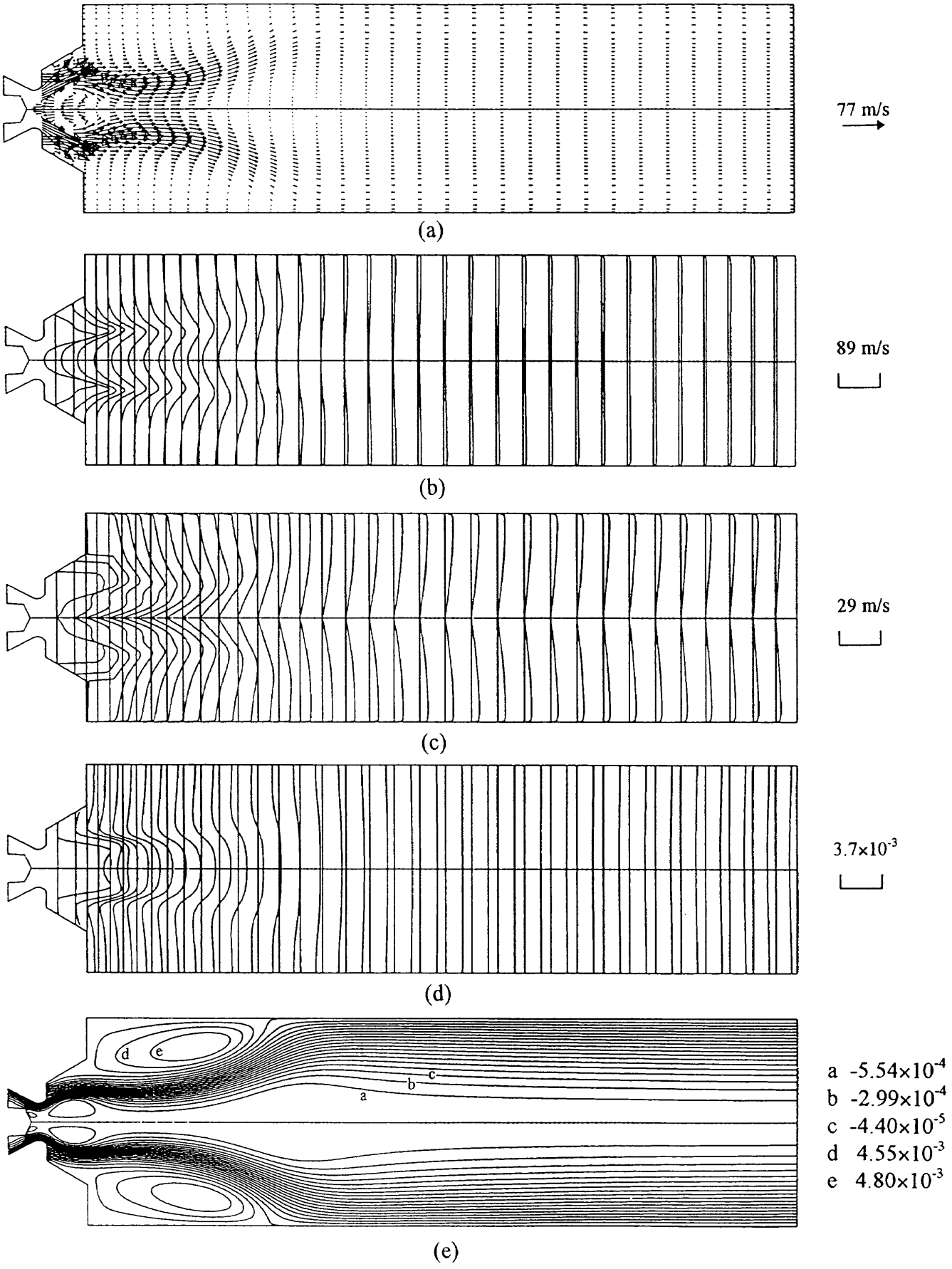

Fig. 22 Predicted results with the standard κ-ε model for Case 5 (a) velocity vectors, (b) axial velocity, (c) tangential velocity, (d) fuel concentration, (e) stream functions

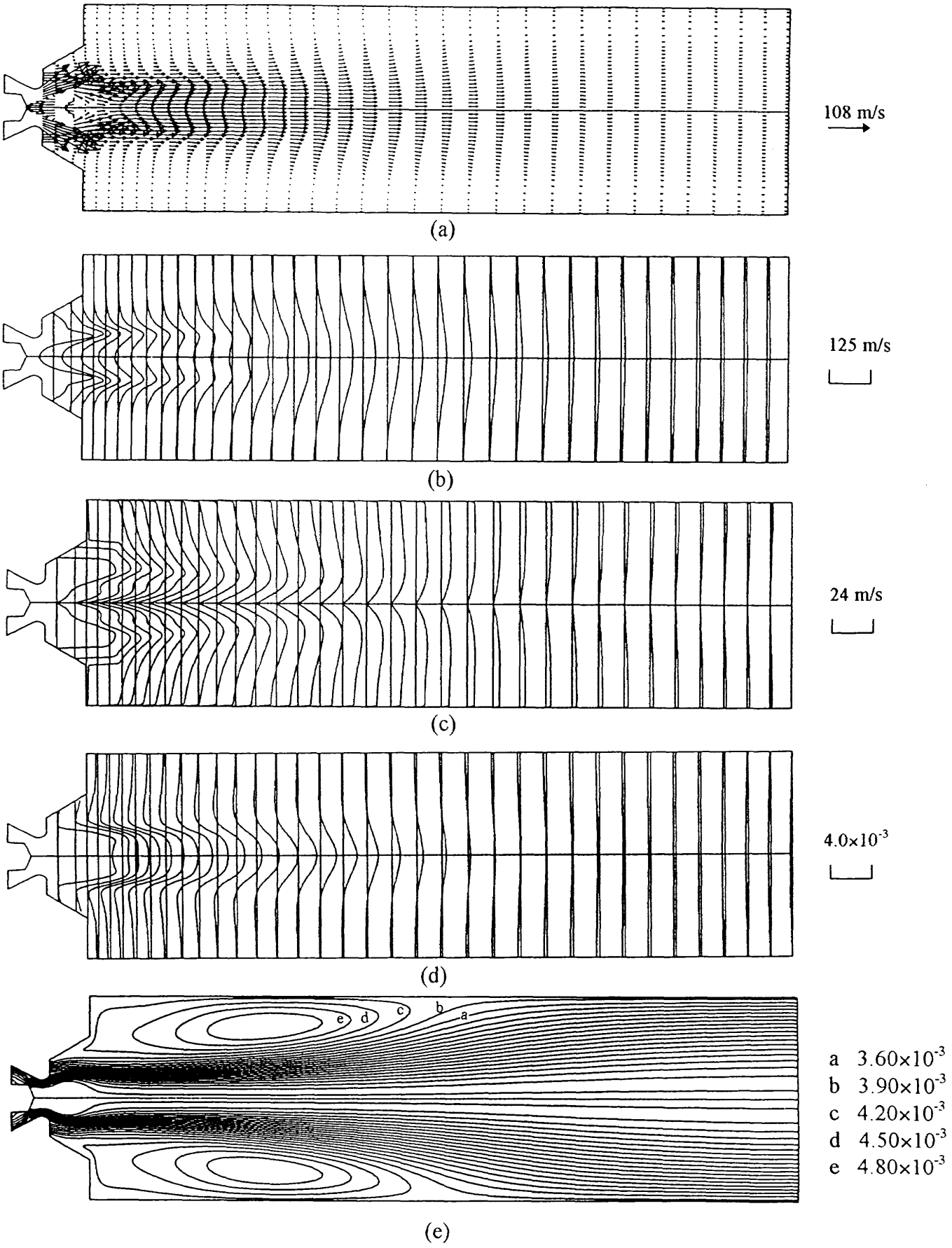

Fig. 23 Predicted results with the standard κ-ε model for Case 6 (a) velocity vectors, (b) axial velocity, (c) tangential velocity, (d) fuel concentration, (e) stream functions

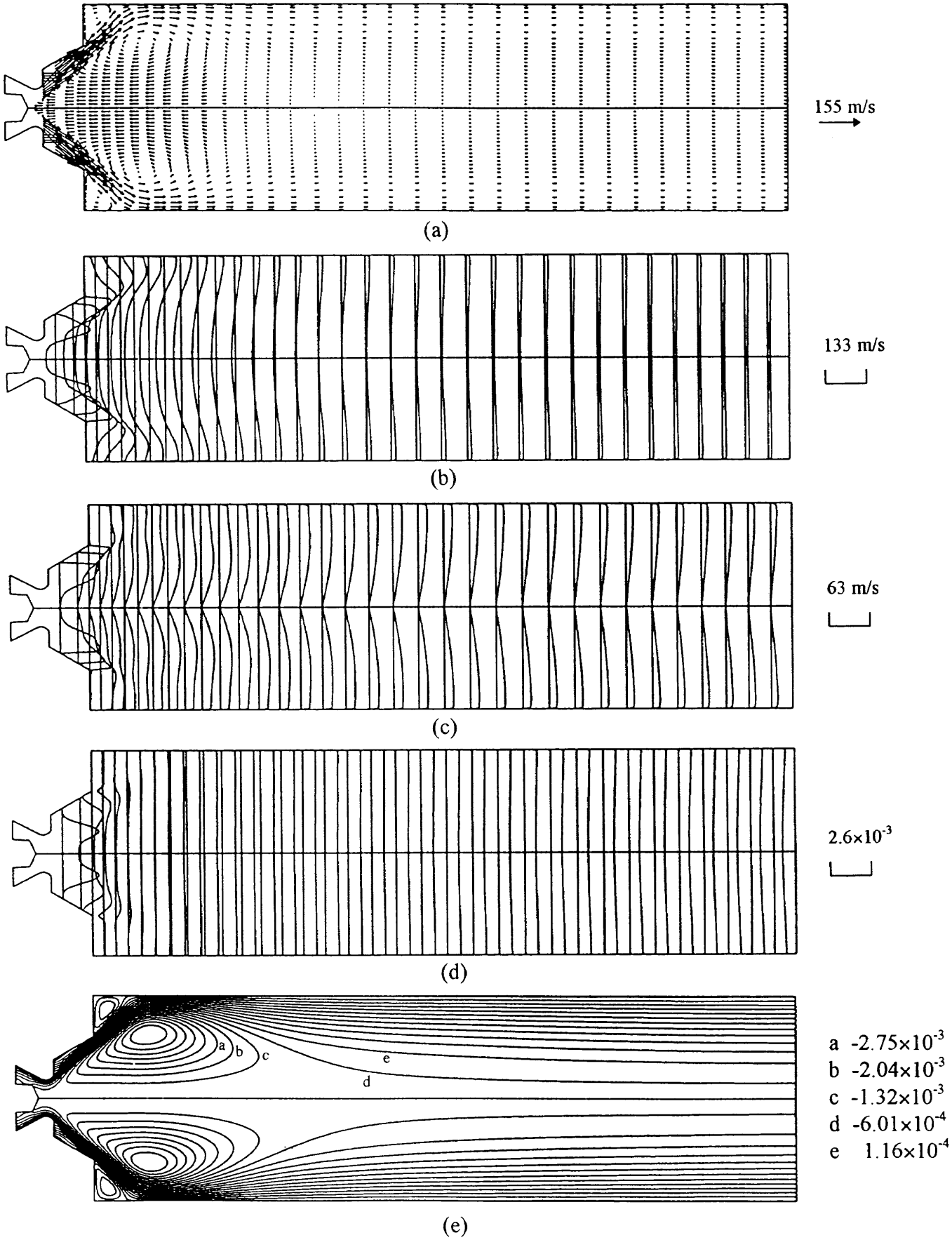

Fig. 24 Predicted results with the standard κ-ε model for Case 7 (a) velocity vectors, (b) axial velocity, (c) tangential velocity, (d) fuel concentration, (e) stream functions

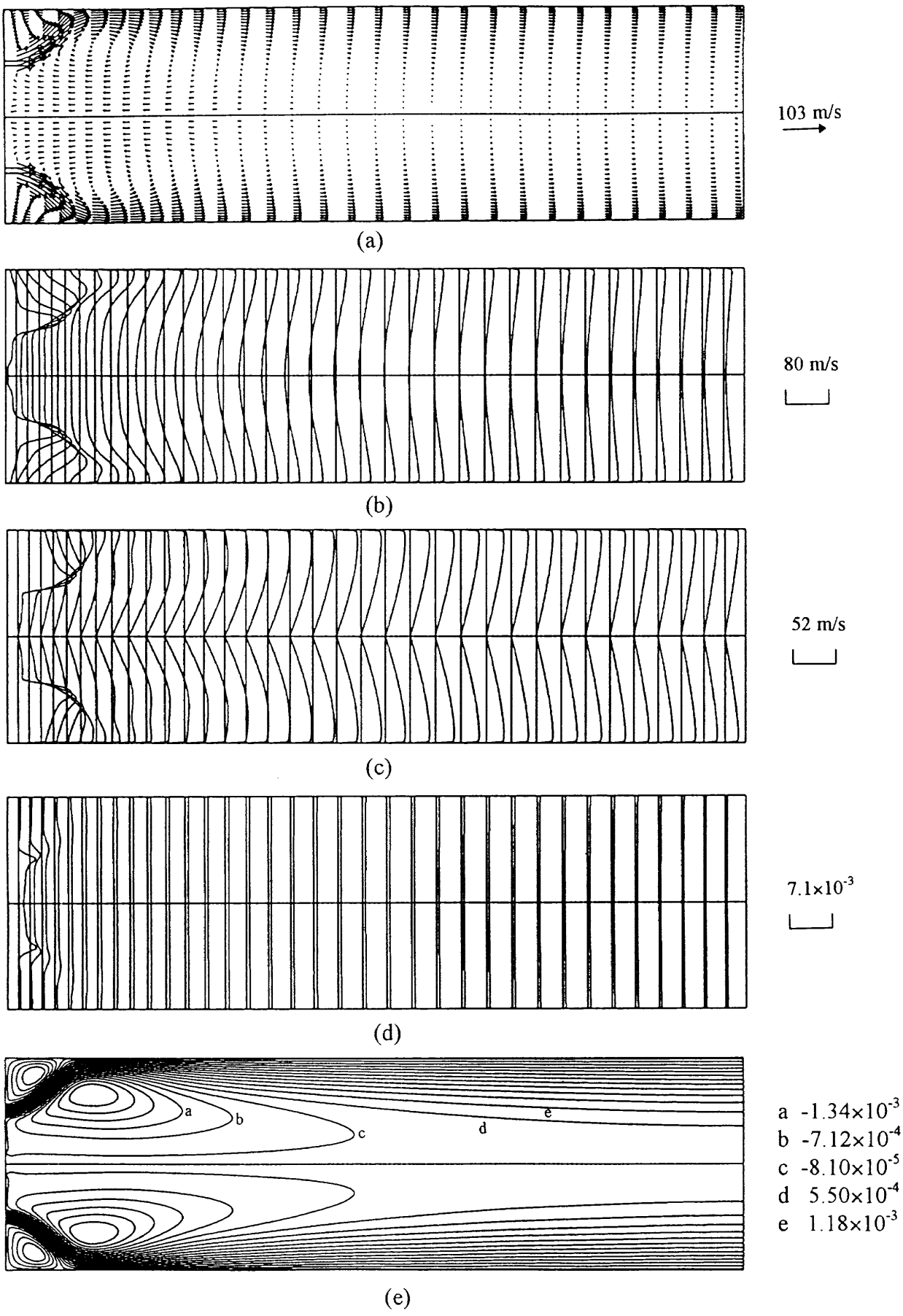

Fig. 25 Predicted results with the standard κ-ε model for Case 9 (a) velocity vectors, (b) axial velocity, (c) tangential velocity, (d) fuel concentration, (e) stream functions

TECHNICAL REPORT OF NATIONAL
AEROSPACE LABORATORY
TR-1318T

航空宇宙技術研究所報告1318T号（欧文）

平成9年1月発行

発行所　科学技術庁航空宇宙技術研究所
東京都調布市深大寺東町7−44−1
電話（0422）47−5911〒182
印刷所　株式会社三興印刷
東京都新宿区西早稲田2−1−18

Published by
NATIONAL AEROSPACE LABORATORY
7-44-1 Jindaijihigashi-Machi, Chofu, Tokyo
JAPAN

Printed in Japan